100 mM with DMSO. Cytochalasin D was from Sigma-Aldrich and stocked in 10 mM with DMSO.

Generation of deletion mutant of human SSTR4. Full-length human SSTR4 construct in pCMV6-Entry vector (SSTR4WT-FLAG) was obtained from OriGene Technologies Inc. (Rockville, MD, USA). Human SSTR4 with deleted C-terminal cytoplasmic region (SSTR4ΔC-FLAG) was made by PCR, using the forward primer (5′-gcgatcgccATGAGCGCC CCCTCGACGCTG-3′) and the reverse primer (5′-acgcgtGAGGA AGCCATAGAGAATGG GGTT-3′), and constructed into *Sgf*I and *Mlu*I sites of pCMV6-Entry vector.

Native polyacrylamide gel electrophoresis. Membrane fraction from MSTO-Mock, MSTO-CD26WT or MSTO-CD26/10Chi cells was extracted with the ProteoExtract Native Membrane Protein Extraction Kit (Invitrogen Dynal AS, Oslo, Norway) according to the manufacturer's instructions. After being precleared with normal goat Ig-crosslinked Dynabeads (VERITAS, Carlsbad, CA, USA), the native membrane extracts were immunoprecipitated with anti-CD26 pAb-crosslinked Dynabeads and eluted with the Elution Buffer of MAG2 Dynabeads Co-Immunoprecipitation Kit (Invitrogen Dynal AS). The eluates were resolved by the Blue Native polyacrylamide gel electrophoresis (PAGE) (Life Technologies Inc.). Analytical gels were stained with SilverQuest (Life Technologies Inc.). Peptide mass mapping was performed by recording peptide mass fingerprints of typical in-gel digests of the corresponding gel bands using tandem mass spectrometry (LC-MS/MS) (nano LCMS-IT-TOF; Shimadzu Biotech, Kyoto, Japan) and subsequently searching the MASCOT database (Matrix Sciences, Boston, MA, USA).

Coimmunoprecipitation, immunoblotting and lipid raft fractioning. To study the interaction between CD26 and SSTR4 using MPM cells, membrane fraction from indicated cells was extracted and coimmunoprecipitation experiments were conducted as described above. To examine the interacting domains through the use of mutant proteins, HEK293 cells were transfected with full-length human CD26, CD26-CD10 chimaeric receptor, SSTR4WT-FLAG or SSTR4ΔC-FLAG expressing plasmids, using Lipofecatmine2000 reagent. Membrane fraction was prepared as described above. After being precleared with normal mouse Ig-conjugated resin, the fractions were immunoprecipitated with anti-FLAG M2 affinity resin and eluted with FLAG peptide. The eluates in sample buffer (1% SDS, 6 M urea, 150 mM NaCl, 1 mM EDTA, 50 mM Tris (pH 8.0)) were then submitted to SDS–PAGE under reducing conditions and western blot analysis using the indicated specific antibodies. To obtain the lipid raft membrane fraction, after stimulation with control IgG or humanised anti-CD26 mAb by crosslinking with anti-Fcγ for 10 min, MSTO-CD26WT cells (each, 1×10^8) were lysed on ice with 1 ml 1% Triton X-100 and 1 mM PMSF in MNE buffer (25 mM MES (pH 6.5), 150 mM NaCl, 5 mM EDTA), followed by sucrose-gradient ultracentrifugation as described previously (Ishii *et al*, 2001). For immunoprecipitation of the pooled lipid raft fractions, fractionated lipid rafts (collection of fraction number 3–5) were lysed at 4 °C for 30 min with 1% *N*-octyl-β-D-glucoside (Nakarai Tesuque, Inc., Kyoto, Japan), and subjected to immunoprecipitation experiments, followed by SDS–PAGE and western blot analyses.

Small interference RNA. Knockdown experiments in MPM cell lines were achieved by transiently transfecting cells with the indicated specific small interference RNAs (siRNAs) or control siRNA (csi), purchased from Sigma-Aldrich. The target sequences of specific siRNA are shown in Supplementary Table. Transfection of siRNA into MPM cells was conducted using the Xfect siRNA Transfection Reagent (Takara Bio Inc., Shiga, Japan). After 48 h of transfection, cells were subjected to the corresponding experiments.

Cell migration, invasion and colony formation assays. For cell migration assay, cells (500 μl of 1×10^5 per ml in 0.1% FBS-RPMI1640) were seeded onto uncoated filters in a 24-well Transwell chamber (8-μm pore size; Costar, Corning, NY, USA) with 750 μl of FBS fresh medium in the lower cell, and allowed to migrate for 24 h at 37 °C in 100% humidifier. The cells that migrated to the underside of the filter were stained with crystal violet and images under brightfield microscopy were captured with an Olympus digital camera DP21 attached to an Olympus BX43 microscope using the CellSens software (Olympus, Tokyo, Japan). Crystal violet-stained cells were counted in five fields per filter using the ImageJ software (The National Institutes of Health). For cell invasion assay, cells (500 μl of 1×10^5 per ml in 0.1% FBS-RPMI1640) were seeded onto filters of a 24-well Transwell chamber that were coated with Matrigel (BD Biosciences) with 750 μl of FBS fresh medium in the lower cell. Invasion of the cells through the Matrigels to the underside of the filter was assessed 24 h later by staining with crystal violet and counting by the same method as in the migration assay. Soft-agar colony formation was assayed using the CytoSelect Cell Transformation Assay kit (Cell Biolabs, Inc., San Diego, CA, USA). Cells (1×10^3) were incubated 7 days in a semisolid agar medium containing the indicated antibody or reagents before being solubilised and detected by using the provided MTT solution in iMark microplate absorbance reader (absorbance at 570 nm) (Bio-Rad Laboratories, Hercules, CA, USA).

***In vivo* evaluation of tumour growth.** Female CB17/Icr-*Prkdc*^{scid}/CrlCrlj mice (SCID mice) were purchased from Charles River Laboratories Japan Inc. (Yokohama, Japan) for experimental animals and housed in a specific pathogen-free facility in micro-isolator cages. Mice were used at 8–12 weeks. SCID mice were injected i.p. with 1×10^5 luciferase-expressing MSTO-Mock, MSTO-CD26WT or MSTO-CD26/10Chi cells (each cohort, $n = 20$). For *in vivo* bioluminescence imaging (BLI), mice were given an i.p. injection of 150 mg kg^{-1} body weight of D-luciferin (Wako Pure Chemical Industries, Osaka, Japan) and then anaesthetised with isoflurane gas. The mice were imaged using Caliper IVIS Lumina II *In Vivo* Imaging System (Perkin-Elmer, Waltham, MA, USA) to assess bioluminescence 10 min after injection of the substrate. Imaging data were analysed with the Caliper Living Image software (Perkin-Elmer) and indicated as total flux of photons per second. Mice demonstrating more than 1×10^9 photons per second or reaching end of the observation periods are euthanised.

Confocal microlaser microscopy. For detection of colocalisation between CD26 and SSTR4 in MESO1 and JMN cells, cells were preincubated in collagen-coated 8-well chamber slide glass cells (Iwaki, Tokyo, Japan), and fixed with 4% paraformaldehyde in PBS (Nakarai Tesque, Inc.). After being washed with ice-cold PBS, cells were blocked with normal goat and rabbit IgG (Santa Cruz Biotechnology Inc.), followed by incubation with Alexa Fluor 488-conjugated anti-CD26 pAb and Alexa Fluor 594-conjugated anti-SSTR4 pAb (each at a concentration of 5 μg ml^{-1}). After being washed with ice-cold PBS, slides were mounted with Prolong Gold antifade reagent with DAPI (Molecular Probes, Eugene, OR, USA). Confocal microscopy was performed with an Olympus IX70 confocal microscope with 60 objective lenses (Olympus), using laser excitation at 496 and 568 nm. The widths of Alexa Fluor 488 and 594 emission channels were set to maximise specificity.

Tissue samples and immunohistochemistry. Fifty MPM tissues were obtained from patients who had undergone biopsy or surgery at Okayama Rosai Hospital (Okayama, Japan) or National Hospital Organization Yamaguchi-Ube Medical Center (Yamaguchi, Japan) between 1998 and 2009. Histological sections from the mesothelioma patients were previously examined and classified into epithelioid, sarcomatoid and biphasic subtypes, according to the

World Health Organization histological classification by three independent pathologists (Takeshima *et al*, 2009), who were blinded to the results of the studies discussed in this article. Immunohistochemistry staining of 50 MPM tissues for CD26 and SSTR4 was performed and evaluated as described previously (Aoe *et al*, 2012).

Assessment of anti-tumour activity of SSTR4 agonist and humanised anti-CD26 mAb in mice. To assess the effect of SSTR4 agonist and humanised anti-CD26 mAb against tumorigenicity, JMN cells (1×10^6) were inoculated s.c. into the left flank of SCID mice. Mice were treated with i.p. injection of control human Ig or humanised anti-CD26 mAb (10 μg per dose) in the presence of SSTR4 agonist (20 μM per dose) or solvent control on the seventh day after cancer cell inoculation, at a time when the tumour mass became visible (5 mm in size). Each antibody or agonist was given three times per week. Each cohort was examined with $n = 20$. Tumours were measured every 4 days using a vernier caliper, and the volume was calculated according to the formula: $1/6 \times \text{length} \times \text{square width}$. For assessment using systemic xenograft model, SCID mice were injected i.p. with 1×10^5 luciferase-expressing JMN cells. Mice were treated with i.p. injection of control human Ig or humanised anti-CD26 mAb (10 μg per dose) in the presence of SSTR4 agonist (20 μM per dose) or solvent control on the next day after cancer cell inoculation. Each antibody or agonist was given three times per week. Each cohort was examined with $n = 20$. Tumour growth was evaluated with BLI every 1 week.

Study approval. Human study protocols were approved by the Ethics Committees at Juntendo University, and at Keio University. Informed consent was obtained from all patients according to the format of the institutional review board at Okayama Rosai Hospital and National Hospital Organization Yamaguchi-Ube Medical Center. All studies on human subjects were carried out according to the principles set out in the Declaration of Helsinki. Animal experiments were conducted following protocols approved by the Animal Care and Use Committees at Juntendo University.

Statistical analysis. All experiments were performed in triplicates and repeated at least three times. Data were expressed as mean values ± s.e.m. (standard error of the mean) and analysed by one-way or two-way ANOVA followed by the Tukey–Kramer *post hoc* test. The level of significance was $P < 0.05$. The calculations were conducted using the Prism6.0 software (GraphPad Software, Inc., La Jolla, CA, USA).

RESULTS

Cytoplasmic region of CD26 has an important role in tumour cell activity of MPM cells. We previously showed that CD26-mediated tumour cell proliferation of T-lymphoma and MPM cell lines was exerted *via* β1 integrin, in relation to the process of cell adhesion (Sato *et al*, 2005; Okamoto *et al*, 2014). Meanwhile, with the proximal signalling events associated with the cytoplasmic region of CD26 being shown in normal human T lymphocytes (Ohnuma *et al*, 2007), it is conceivable that similar CD26-mediated proximal events may have a role in MPM cell biology. To define the crucial role of the CD26 cytoplasmic region in regulating migratory, invasive or proliferative activity of MPM cells, we used a mutant construct of CD26 in which its cytoplasmic region was replaced with that of human CD10 (CD26-CD10 chimaeric receptor), which was shown to abrogate CD26-mediated costimulation in T cells (Ohnuma *et al*, 2007). CD10, as is the case with CD26, is a type II transmembrane glycoprotein with a relatively short cytoplasmic tail containing signal sequence that has an expected membrane topology similar to CD26 (Ogata *et al*, 1989; Maguer-Satta *et al*, 2011). We then transfected CD26-negative parental MSTO cells with full-length human CD26 or CD26-CD10 chimaeric receptor to establish MSTO-CD26WT or MSTO-CD26/10Chi, respectively (Supplementary Figure S1A). As shown in Figure 1A, a significant increase in migration was observed in MSTO-CD26WT as compared with MSTO-Mock ($P < 0.0001$) or MSTO-CD26/10Chi ($P < 0.0001$). Similarly, an increase in invasion was also observed in MSTO-CD26WT as compared with MSTO-Mock or MSTO-CD26/10Chi (Figure 1B). To study the process of tumour formation in MPM cells, we conducted colony formation assay as a model of anchorage-independent cell growth. As shown in Figure 1C, a significant increase in colony formation was observed in MSTO-CD26WT as compared with MSTO-Mock ($P < 0.0001$) or MSTO-CD26/10Chi ($P < 0.0001$). To extend the above *in vitro* results to *in vivo* experimentation, we conducted the cell growth assay using tumour-transplant mice. A significant increase in *in vivo* tumour growth was observed with MSTO-CD26WT as compared with MSTO-Mock ($P < 0.0001$) or MSTO-CD26/10Chi ($P < 0.0001$) (Figure 1D). These results suggest that the cytoplasmic region of CD26 is important for CD26 function in such biological processes of MPM as cell migration, invasion and anchorage-independent cell growth as well as *in vivo* tumour growth using xenograft mouse model.

CD26 associates with SSTR4 *via* their respective cytoplasmic regions. To define the molecular details involved in the critical role of the CD26 cytoplasmic region, we used affinity purification and LC-MS/MS to identify the proteins that are associated with the CD26 cytoplasmic domain. In these experiments, membrane fractions of MSTO-Mock, MSTO-CD26WT or MSTO-CD26/10Chi were harvested in native conditions and subjected to affinity purification using anti-CD26 pAb. LC-MS/MS analysis suggested that the CD26 cytoplasmic region copurified with CD26, actin, TRAK2 (trafficking protein, kinesin binding 2), PEX1 (peroxin1), ribosomal proteins (S2, S3 and S4) and SSTR4 (lane 2 of Figure 2A). It is expected that CD26 co-precipitates with CD26 itself as CD26 forms homodimers in cell membrane (Chien *et al*, 2004). To determine whether these proteins are present in MPM cells, we conducted a conventional western blotting analysis using total cell lysates of MSTO-Mock, MSTO-CD26WT or MSTO-CD26/10Chi. While SSTR4 was detected, TRAK2 and PEX1 of MSTO cells was not detected in 50 μg of each lysate, suggesting that SSTR4 is a primary CD26-interacting protein involved in MPM cell regulation. In addition, as actin and ribosomal proteins (S2, S3 and S4) exist abundantly in cells, the presence of these proteins in the copurified complex might not be specific to CD26. We have therefore confirmed the presence of SSTR4 in the CD26-interacting complex by western blotting analysis. As shown in Figure 2B, SSTR4 coimmunoprecipitated with CD26 in MSTO-CD26WT (lane 2), but not MSTO-Mock or MSTO-CD26/10Chi (lanes 1 or 3, respectively). In addition, the association of endogenous CD26 and SSTR4 was confirmed by coimmunoprecipitation experiments using JMN or MESO1 cells that express CD26 endogenously (lanes 2 or 3 of Figure 2C, respectively, and Supplementary Figure S1B). To confirm the above findings in living cells, we performed immunocytochemical analysis using confocal laser microscopy. As shown in Figure 2D, the association of endogenous CD26 and SSTR4 was clearly observed in JMN or MESO1 cells. These results indicate that the interaction between CD26 and SSTR4 occurs not only in MPM cells with exogenous CD26 expression, but also in MPM cells with natively expressed CD26.

Previous work has demonstrated that the C-terminal intracytoplasmic tail of SSTR4 is essential for homo- and heterodimerisation (Somvanshi *et al*, 2009). To determine whether the C-terminal intracytoplasmic tail of SSTR4 is required for binding

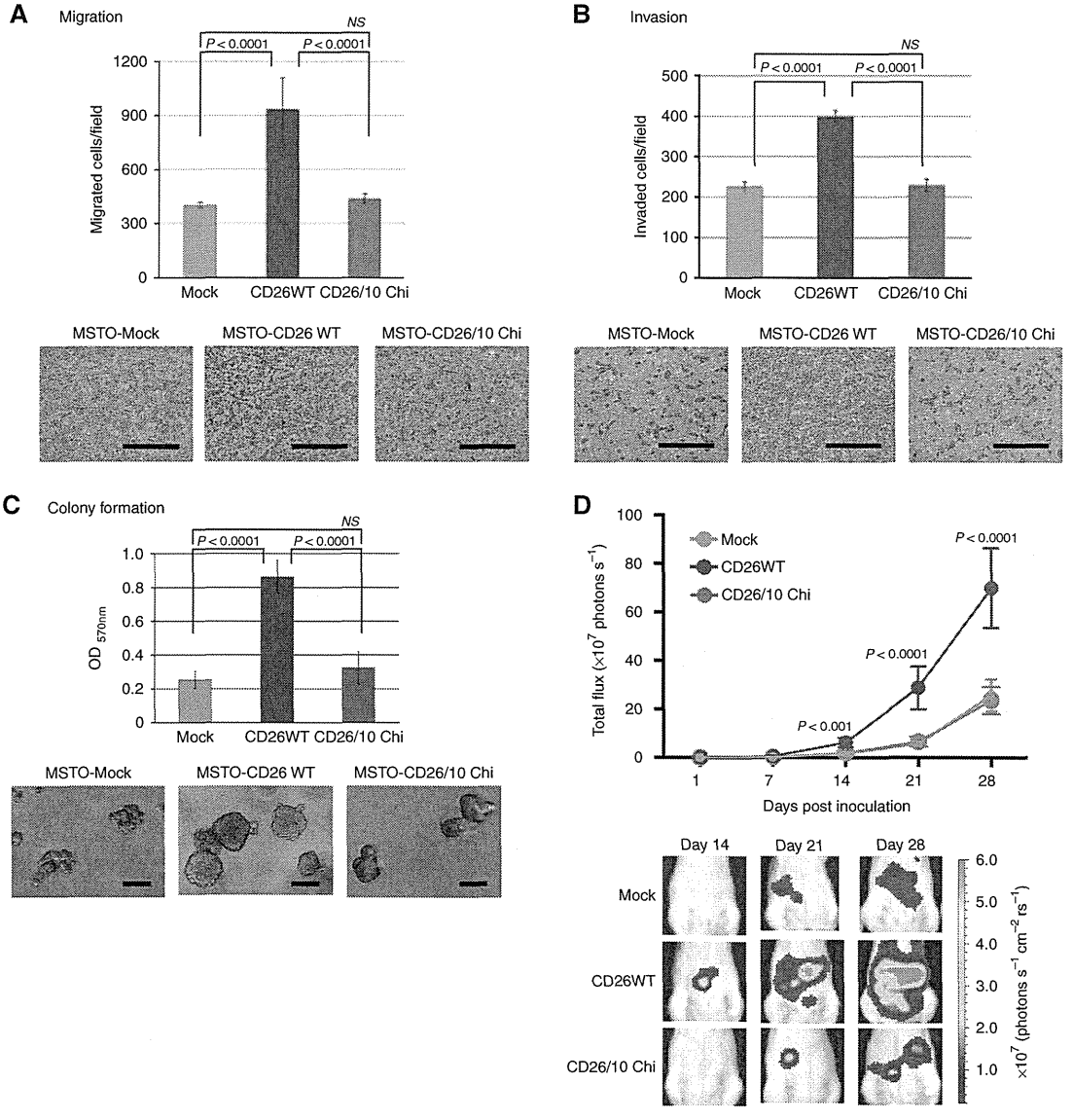

Figure 1. The cytoplasmic region of CD26 is required for cell migration, invasion and colony formation. (**A**) Cells were seeded on top of a Boyden chamber. The number of cells that migrated through the uncoated filter in the lower chamber was counted. The mean number of cells per field was determined from five fields per filter (mean ± s.e.m.; $n=5$ experiments with triplicates). A significant increase in MSTO-CD26WT is indicated as $P<0.0001$ (*vs* MSTO-Mock or MSTO-CD26/10Chi), as calculated by ANOVA with Tukey–Kramer *post hoc* test. NS denotes 'not significant'. Representative microphotographs of cells migrating through the filter were shown in the lower panels (crystal violet staining). Scale bars indicate 200 μm. (**B**) Cells were seeded on top of Matrigel-coated chamber inserts. The number of cells that invaded through the Matrigel in the lower chamber was counted. The mean number of cells per field was determined from five fields per filter (mean ± s.e.m.; $n=5$ experiments with triplicates). A significant increase in MSTO-CD26WT is indicated as $P<0.0001$ (*vs* MSTO-Mock or MSTO-CD26/10Chi), as calculated by ANOVA with Tukey–Kramer *post hoc* test. NS denotes 'not significant'. Representative microphotographs of cells invading through the filter were shown in the lower panels (crystal violet staining). Scale bar indicates 200 μm. (**C**) Cells were plated in a cell suspension agar matrix between layers of base agar matrix. After 1 week, the agar matrix was solubilised and the cells were stained with MTT solution. Absorbance at 570 nm was measured (mean ± s.e.m.; $n=5$ experiments with triplicates). A significant increase in MSTO-CD26WT is indicated as $P<0.0001$ (*vs* MSTO-Mock or MSTO-CD26/10Chi), as calculated by ANOVA with Tukey–Kramer *post hoc* test. NS denotes 'not significant'. Representative microphotographs of cells grown in soft agar just before solubilisation to indicate cell size and morphology were shown in the lower panels (phase-contrast imaging). Original magnification, × 8. Scale bars indicate 50 μm. (**D**) SCID mice were injected i.p. with 1×10^5 luciferase-expressing MSTO-Mock, MSTO-CD26WT or MSTO-CD26/10Chi cells. Tumour growth was measured by *in vivo* bioluminescence photometry, with imaging data of each cohort being indicated as total flux of photons per second (mean ± s.e.m.; $n=20$). A significant increase in MSTO-CD26WT is indicated as $P<0.0001$ (*vs* MSTO-Mock or MSTO-CD26/10Chi), as calculated by ANOVA with Tukey–Kramer *post hoc* test. Representative optical bioluminescence imaging of each cohort mice was shown with intensity of luminescence as heat maps in the lower panels. The full colour version of this figure is available at *British Journal of Cancer* online.

to CD26, we constructed the C-terminal deletion mutant of FLAG-tagged SSTR4 (SSTR4ΔC-FLAG), and coimmunoprecipitation experiments were then conducted. As shown in Figure 2E, the full-length SSTR4 (SSTR4WT-FLAG) co-precipitated with CD26WT (lane 2), but not with CD26/10Chi (lane 4), while SSTR4ΔC-FLAG did not co-precipitate with CD26WT (lane 3), nor with CD26/10Chi (lane 5). Taken together with the results described earlier, our data indicate that the association between CD26 and SSTR4 requires for their respective cytoplasmic domains.

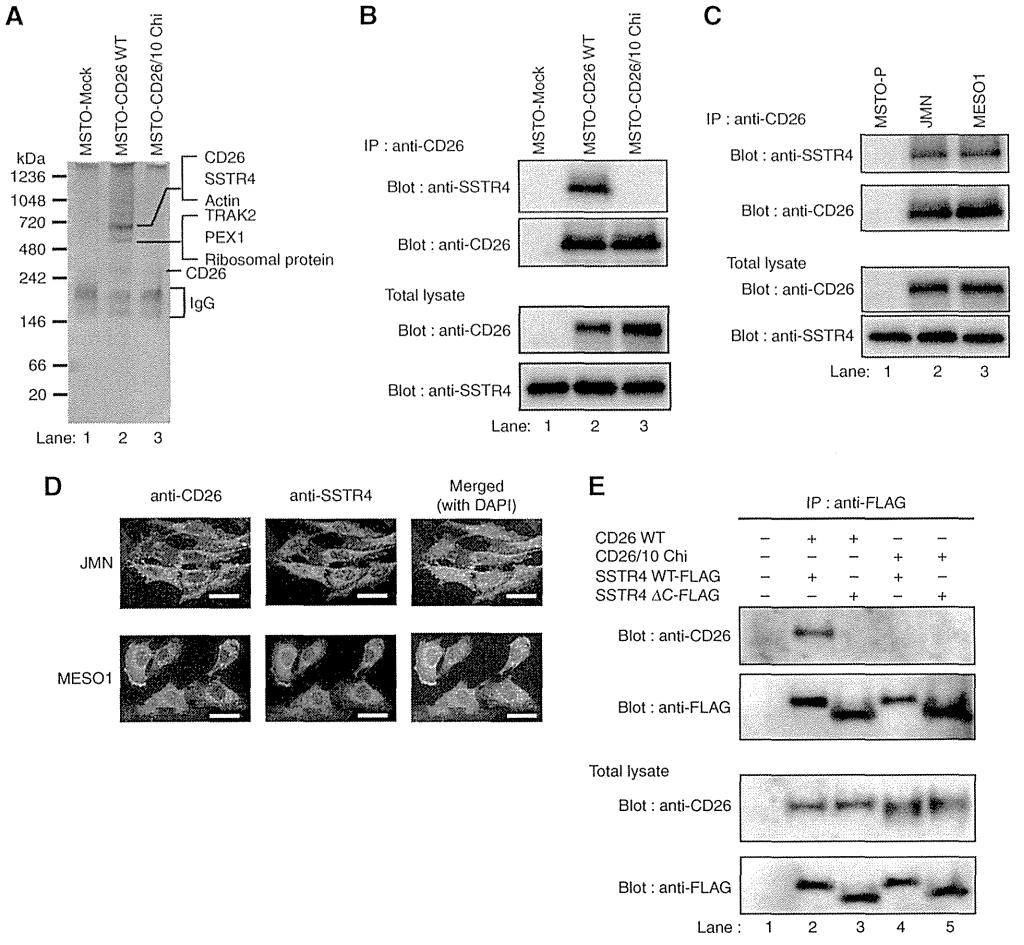

Figure 2. CD26 interacts with somatostatin receptor 4 (SSTR4) in MPM cells. (**A**) Immunoaffinity purification of CD26-containing proteins. Membrane fractions of MSTO-Mock, MSTO-CD26WT or MSTO-CD26/10Chi were extracted in a native condition. After being precleared with normal goat immunoglobulin (Ig) crosslinked Dynabeads, the native membrane extracts were immunoprecipitated with anti-CD26 pAb-crosslinked Dynabeads and eluted. The eluates were resolved by the Blue Native PAGE and sliver stained. The protein bands were retrieved and analysed by tandem mass spectrometry. The determined proteins were indicated in the right of the panel. Similar results were obtained in three independent experiments. (**B**) Immunoprecipitation assay using membrane extractions from MSTO-Mock, MSTO-CD26WT or MSTO-CD26/10Chi. After being precleared with normal goat Ig crosslinked Dynabeads, the membrane extracts were immunoprecipitated by the same method as shown in (**A**). The eluates were resolved by SDS–PAGE, and immunoblotted using anti-CD26 or anti-SSTR4 antibodies (upper two panels). Total lysates from each cell type were resolved by SDS–PAGE, and immunoblotted using anti-CD26 or anti-SSTR4 antibodies (lower two panels). SSTR4 is co-precipitated with CD26WT, but not with CD26/CD10 chimaeric protein (upper panel). Similar results were obtained in three independent experiments. (**C**) Immunoprecipitation assay using membrane extractions from parental MSTO-H211 (MSTO-P), JMN or H-MESO-1 (MESO1) cell lines. The membrane extracts were immunoprecipitated and immunoblotted by the same method as shown in (**B**). SSTR4 is co-precipitated with natively expressing CD26 molecules (upper panel). Similar results were obtained in three independent experiments. (**D**) Colocalisation of CD26 with SSTR4. JMN or MESO1 cells were fixed using 4% paraformaldehyde-PBS, and stained with Alexa Fluor 488-conjugated anti-CD26 pAb and Alexa Fluor 594-conjugated anti-SSTR4 pAb. Stained cells were mounted using Prolong Gold antifade reagent with DAPI. Observations were made on 10–15 cells in each of three different experiments using confocal laser microscopy. The micrographs are representative of >75% of the cells observed. CD26 and SSTR4 are observed as punctate coexpression on the cell surface. Original magnification, ×200. Scale bars indicate 25 μm. (**E**) Association of CD26 with SSTR4 *via* their respective C-terminal region. After being precleared using normal mouse Ig and protein G resin, membrane extracts from HEK293 cells transiently expressing full-length CD26 (CD26WT), CD26-CD10 chimaeric receptor (CD26/10Chi), FLAG-tagged full-length SSTR4 (SSTR4WT-FLAG) or FLAG-tagged SSTR4 with deleted C-terminal cytoplasmic tail (SSTR4ΔC-FLAG) were immunoprecipitated with anti-FLAG affinity resin. Immunocomplexes were then immunoblotted using anti-CD26 or anti-FLAG antibodies (upper two panels). Total lysates from each cell were resolved by SDS–PAGE, and immunoblotted using anti-CD26 or anti-FLAG antibodies (lower two panels). Co-precipitation is observed in CD26WT and SSTR4WT, but not in CD26WT and SSTR4ΔC, CD26/10Chi and SSTR4WT, or CD26/10Chi and SSTR4ΔC (upper panel). Similar results were obtained in three independent experiments. The full colour version of this figure is available at *British Journal of Cancer* online.

Cytostatic effects of SSTR4 agonist are enhanced following suppression of CD26 expression. Since previous reports have shown that SSTR4 agonists mediate growth inhibition of neuroendocrine cells (Patel, 1999; Weckbecker *et al*, 2003), we next examined the effect of SSTR4 on MPM cell migration, invasion and colony formation. For this purpose, knockdown experiments using siRNA against SSTR4 were conducted in MPM cells. Expression of CD26 or SSTR4 was determined by western blotting analysis of cell lysates of MSTO-Mock, MSTO-CD26WT or MSTO-CD26/10Chi in the presence of control siRNA or two different sequences of SSTR4-siRNAs (si-1 or si-2) (Supplementary Figure S2A). As shown in Figure 3A, inhibition of migration, invasion and colony formation was abrogated in MSTO-Mock ($P<0.0001$) and MSTO-CD26/10Chi ($P<0.0001$) in the presence

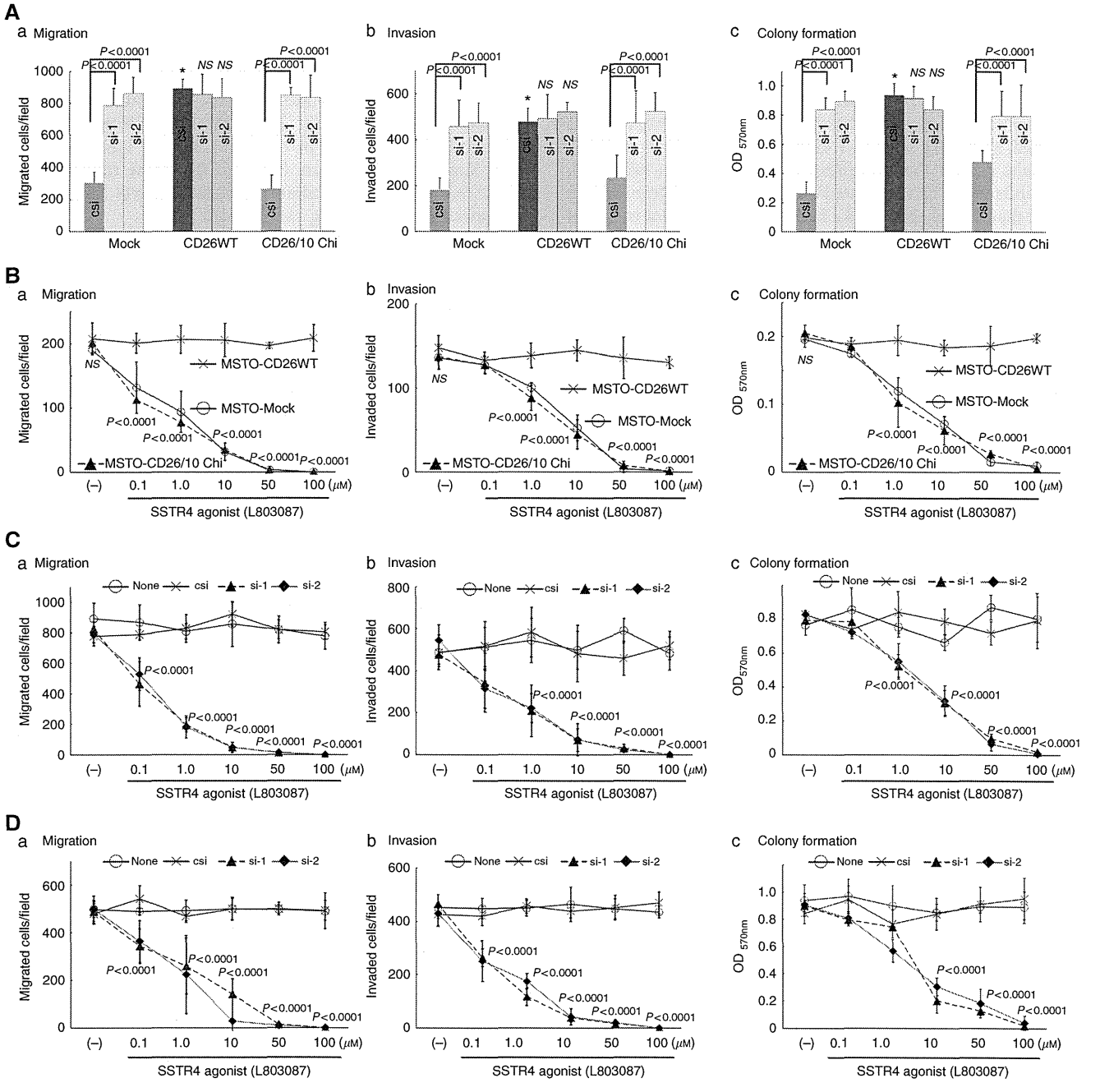

Figure 3. SSTR4-mediated cytostatic effects are inhibited in the presence of CD26. (**A**) MSTO-Mock, MSTO-CD26WT or MSTO-CD26/10Chi cells were transfected with two different siRNAs against SSTR4 (si-1 or si-2) or control siRNA (csi). After 48 h of transfection, cell migration (panel a), invasion (panel b) or colony formation assays (panel c) were conducted by the same methods as in Figure 1 (mean ± s.e.m.; $n = 5$ experiments with triplicates), with results being shown in bar graphs (MSTO-Mock (red bar), MSTO-CD26WT (blue bar) or MSTO-CD26/10Chi (green bar)). A significant increase in si-1 or si-2 in MSTO-Mock or MSTO-CD26/10Chi cells is indicated as $P<0.0001$ (*vs* the corresponding csi). A significant increase in csi of MSTO-CD26WT cells (*) is indicated as $P<0.0001$ (*vs* csi of MSTO-Mock or MSTO-CD26/10Chi). NS denotes 'not significant'. *P*-values are calculated by ANOVA with Tukey–Kramer *post hoc* test. (**B**) Using MSTO-Mock, MSTO-CD26WT or MSTO-CD26/10Chi cells adapted to the serum-reduced condition, cell migration (panel a), invasion (panel b) or colony formation assays (panel c) were conducted by the same methods as in Figure 1 (mean ± s.e.m.; $n = 5$ experiments with triplicates). The SSTR4 agonist L803087 at the indicated concentrations or DMSO as a solvent control was added to the assays. $P<0.0001$ *vs* those in MSTO-Mock or MSTO-CD26/10Chi at respective concentrations of L803087 is calculated by ANOVA with Tukey–Kramer *post hoc* test. NS denotes 'not significant'. (**C**, **D**) Knockdown of endogenous CD26 induces inhibitory effects of SSTR4 agonist in JMN or MESO1 cells. After being adapted to the serum-reduced condition, endogenous CD26-expressing JMN (**C**) or MESO1 (**D**) cells were transfected with two different siRNAs against CD26 (si-1 or si-2), control siRNA (csi) or transfection reagent alone (none). After 48 h of transfection, cell migration (panels a), invasion (panels b) or colony formation assays (panels c) were conducted by the same methods as in Figure 1 (mean ± s.e.m.; $n = 5$ experiments with triplicates). The SSTR4 agonist L803087 at the indicated concentrations or DMSO as a solvent control was added to the assays. A significant decrease in si-1 or si-2 is indicated as $P<0.0001$ (*vs* the corresponding csi or none), as calculated by ANOVA with Tukey–Kramer *post hoc* test. The full colour version of this figure is available at *British Journal of Cancer* online.

of SSTR4-siRNAs. For cells treated with control siRNA (csi), an increase in migration, invasion and colony formation was observed in MSTO-CD26WT (* in panels a–c of Figure 3A) as compared with MSTO-Mock ($P<0.0001$) or MSTO-CD26/10Chi ($P<0.0001$), similar to results seen in Figure 1A–C. However, the enhancement in cellular activities seen in MSTO-CD26WT was not affected by SSTR4-siRNAs (NS in panels a–c of Figure 3A). These results suggest that coexpression of SSTR4 with full-length CD26 inhibits the SSTR4-mediated cytostatic effects. Meanwhile, it is possible that SSTR4 agonist-like factors may be present in FBS of the culture medium, as SSTRs bind the naturally occurring peptides SST-14 and SST-28 with similar affinity (Bruns *et al*, 1994), affecting cell migration, invasion or colony formation of MSTO-Mock and MSTO-CD26/10Chi (panels a–c of Figure 3A). To exclude the possibility of serum-derived SSTR4 agonistic effect, we established various MPM cell lines that have been adapted to the serum-reduced condition, and conducted cell migration, invasion and colony formation assays in the presence or absence of the specific SSTR4 agonist L803087 (Rohrer, 1998). The expression levels of CD26 or SSTR4 in these adapted MPM cells were confirmed by western blot analysis to be similar to those of respective parental cells (Supplementary Figure S2B). As shown in Figure 3B, levels of cell migration, invasion and colony formation were observed to be equal among MSTO-Mock, MSTO-CD26WT or MSTO-CD26/10Chi (NS at points of medium alone in panels a–c), suggesting that the influence of serum on these cell lines was minimised by the serum-reduced condition. Under this serum-reduced condition, inhibition of migration, invasion and colony formation of MSTO-Mock or MSTO-CD26/10Chi by the SSTR4 agonist was observed in a dose-dependent manner (○ or ▲ in panels a–c, respectively), while inhibition of migration, invasion or colony formation of MSTO-CD26WT in a serum-reduced condition was not observed (× in panels a–c of Figure 3B). These results strongly suggest that SSTR4-mediated cytostatic effects are abrogated in the presence of CD26.

To determine whether SSTR4-mediated cytostatic effects are abrogated in the presence of the association between CD26 and SSTR4, knockdown experiments using siRNA against CD26 were conducted in JMN or MESO1 cell lines. Expression of CD26 or SSTR4 was determined by western blotting analysis of cell lysates of JMN or MESO1 cell lines in the presence of control siRNA (csi) or two different sequences of CD26-siRNAs (si-1 or si-2) (Supplementary Figure S2C). Following knockdown of endogenous CD26, inhibition of migration, invasion and colony formation of JMN cells by SSTR4 agonist in a serum-reduced condition was observed in a dose-dependent manner of L803087 ($P<0.0001$, panels a–c of Figure 3C). Similarly, following knockdown of endogenous CD26 in MESO1 cells adapted to a serum-reduced condition, inhibition of migration, invasion and colony formation by SSTR4 agonist was also observed in a dose-dependent manner of L803087 ($P<0.0001$, panels a–c of Figure 3D). These results indicate that SSTR4-mediated cytostatic effects are strongly elicited by decreased CD26 expression. Taken together, our results strongly suggest that the association of CD26 with SSTR4 impedes the cytostatic signalling of the SSTR4 agonist.

Downstream signalling *via* SHP-2 is required for SSTR4-mediated cytostatic effects. To further clarify the role of the association between CD26 and SSTR4 on SSTR4-mediated cytostatic effects in MPM, we next investigated the molecular basis for downstream signalling events elicited by the SSTR4 agonist. Since previous work indicated that PTPs, SHP-1 or SHP-2 are involved in signalling events of the SSTR family (Patel, 1999; Weckbecker *et al*, 2003; Florio, 2008), we conducted experiments using an SHP inhibitor. As shown in Figure 4A, the SHP-1/2 PTP inhibitor abrogated the inhibitory effect of SSTR4 agonist on cell migration, invasion and colony formation of MSTO-P cells adopted to a serum-reduced condition (panels a–c). To further support the conclusion that SSTR4-mediated cytostatic effects were abrogated by the SHP-1/2 PTP inhibitor, we conducted similar experiments with JMN or MESO1 cells, and found that SSTR4-mediated cytostatic effects in CD26-knockdown cells were abrogated in the presence of the SHP-1/2 PTP inhibitor (panels a–c of Supplementary Figure S3A and B). These results strongly suggest that the SSTR4-mediated cytostatic effects are associated with downstream signalling *via* SHP-1/2 PTPs.

To further characterise the involvement of SHP-1/2 PTPs downstream of SSTR4, we next analysed expression levels of SHP-1 and SHP-2 in various cell lines. As shown in Supplementary Figure S3C, MPM cell lines used in the current study expressed SHP-2, but not SHP-1. These results suggest that SHP-2 PTP is predominantly associated with SSTR4-mediated cytostatic effects in our experimental system. As further support for this conclusion, we next conducted knockdown experiments using siRNAs against SHP-2 in MSTO-Mock cells. Expression of SHP-1/2, SSTR4 and CD26 was determined by western blotting analysis of cell lysates in the presence of control siRNA (csi) or two different sequences of SHP-2-siRNAs (si-1 or si-2). Endogenous SHP-2 was clearly reduced by SHP2-siRNAs without any change in the level of endogenous SSTR4 expression. Endogenous CD26 and SHP-1 were not detected in MSTO-Mock (Supplementary Figure S3D). As shown in Figure 4B, SHP-2-siRNAs clearly abrogated SSTR4-mediated cytostatic effects in MSTO-Mock cells (▲ or ◆ in panels a–c), with dose-dependent inhibition of migration, invasion and colony formation by SSTR4 agonist being observed in a dose-dependent manner (○ or × in panels a–c). Our overall results hence indicate that SSTR4-mediated cytostatic effects in MPM cells are exerted *via* SHP-2 signalling.

SSTR4-mediated cytostatic effects are enhanced *via* lipid raft aggregation induced by humanised anti-CD26 mAb. It has been previously shown that CD26-mediated costimulatory signalling in T cells was exerted *via* lipid raft clustering (Ishii *et al*, 2001; Ohnuma *et al*, 2007). Moreover, it is estimated that SSTR4 is recruited into lipid rafts *via* a palmitoyl membrane anchor site which is located at the cysteine residue of its C-tail region (Patel, 1999). In view of these molecular characteristics of CD26 and SSTR4, to define the molecular events involved in the formation of these critical integrated cell membrane protein–protein complexes, we analysed the molecular clustering induced by lipid raft aggregation in MPM cells treated with humanised anti-CD26 mAb. As shown in Figure 5A, humanised anti-CD26 mAb treatment resulted in increased levels of CD26, SSTR4 and SHP-2 molecules in lipid raft fractions (upper three of right panels) while a non-lipid raft anchored protein, transferrin receptor (TfR), was not aggregated in lipid raft fractions (bottom panels). Furthermore, to examine whether anti-CD26 mAb treatment affects CD26 binding to SSTR4 in lipid rafts, co-precipitation assay was performed using lipid raft fractions. As shown in Figure 5B, CD26 in lipid rafts of MPM cell treated with control IgG was co-precipitated with SSTR4 (lane 1), while CD26 was not co-precipitated with SSTR4 in lipid raft fractions of MPM cells following stimulation with humanised anti-CD26 mAb, despite the presence of SSTR4 in lipid raft fractions (lane 2). These results suggest that SSTR4 and CD26 are associated in lipid rafts, and that anti-CD26 mAb ligates CD26 to cause the release of SSTR4 from CD26 and the clustering of SSTR4 in lipid rafts, hence providing a platform for signalling events associated with multimerisation of SSTR4 molecules, such as SHP-2 activation.

To further evaluate the association of CD26 and SSTR4 *via* lipid raft, we conducted experiments using a lipid raft disturbing reagent, cytochalasin D (Cytoch. D) (Ishii *et al*, 2001). Cytoch. D slightly inhibited cell migration, invasion and colony formation

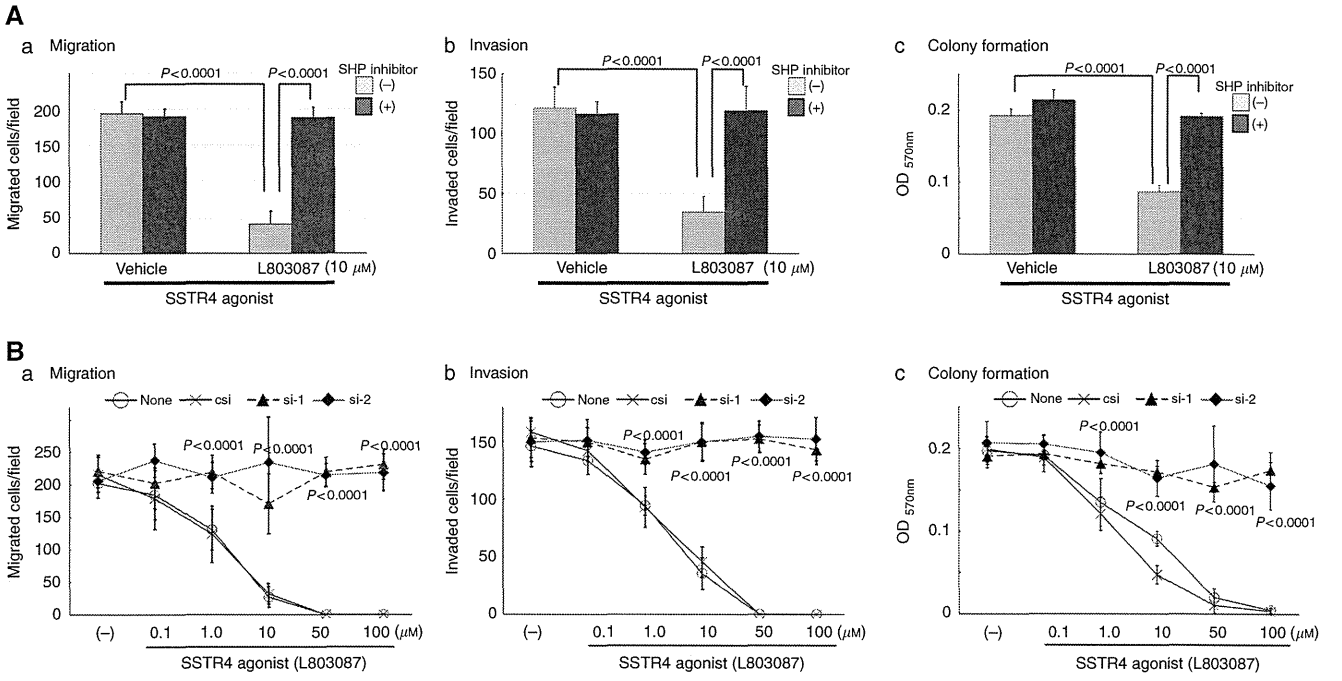

Figure 4. Downstream signalling with SHP-2 has a role in SSTR4-mediated cytostatic effects. (**A**) Endogenous CD26-deficient parental MSTO cells (MSTO-P) adapted to the serum-reduced condition were incubated with 1 μM of SHP-1/2 inhibitor (black bars) or PBS as a solvent control (grey bars) for 30 min, followed by cell migration (panel a), invasion (panel b) or colony formation assays (panel c) in the presence of the SSTR4 agonist L803087 (10 μM) or DMSO as a solvent control (vehicle) (mean ± s.e.m.; $n=5$ experiments with triplicates). A significant suppression in L803087 treatment without SHP-1/2 inhibitor ($P<0.0001$, grey bars) was restored in the presence of SHP-1/2 inhibitor ($P<0.0001$, grey and black bars of L803087), as calculated by ANOVA with Tukey–Kramer *post hoc* test. (**B**) MSTO-P cells adapted to the serum-reduced condition were transfected with two different siRNAs against SHP-2 (si-1 or si-2), control siRNA (csi) or transfection reagent alone (none). After 48 h of transfection, cell migration (panel a), invasion (panel b) or colony formation assays (panel c) were conducted by the same methods as in Figure 1 (mean ± s.e.m.; $n=5$ experiments with triplicates). The SSTR4 agonist L803087 at the indicated concentrations or DMSO as a solvent control was added to the assays. A significant increase in si-1 or si-2 is indicated as $P<0.0001$ (*vs* the corresponding csi or none), as calculated by ANOVA with Tukey–Kramer *post hoc* test.

at the indicated concentration ($P<0.001$) (panels a–c of Figure 5C), as Cytoch. D is a potent inhibitor of actin polymerisation (Brenner and Korn, 1979). However, as shown in panels a–c of Figure 5C, anti-CD26 mAb treatment resulted in enhanced inhibitory effect on cell migration, invasion and colony formation at the indicated concentration ($P<0.0001$), and this inhibitory effect was more profoundly exerted in the presence of the SSTR4 agonist (*, $P<0.0001$). On the other hand, this inhibitory effect of anti-CD26 mAb on cell migration, invasion and colony formation was reversed in the presence of Cytoch. D ($P<0.001$) (panels a–c of Figure 5C). Similar effects of Cytoch. D were observed in cell migration, invasion and colony formation assays using JMN or MESO1 cells (Supplementary Figure S4B or C, respectively). These results indicate that the effect of humanised anti-CD26 mAb on anti-tumour activity is enhanced by SSTR4-mediated activation of SHP-2, which is induced by lipid raft clustering.

Anti-tumour effect of humanised anti-CD26 mAb is enhanced in combination with SSTR4 agonist *in vivo*. To further validate our *in vitro* observations regarding the enhancing effect of humanised anti-CD26 mAb treatment on SSTR4-mediated anti-tumour effect, we conducted *in vivo* experiments using SCID mice transplanted with MPM cells. As shown in Figure 6A and B, humanised anti-CD26 mAb reduced the tumorigenicity of s.c. inoculated JMN (blue line, $P<0.0001$), while this anti-tumour effect was not observed in mice treated with the SSTR4 agonist L803087 alone (green or yellow lines). This *in vivo* anti-tumour effect was enhanced with the combined administration of humanised anti-CD26 mAb and SSTR4 agonist (red line in Figure 6A, $P<0.0001$, and Figure 6B). To further define the *in vivo* effect of the combined treatment of anti-CD26 mAb and SSTR4 agonist, serial BLI study was conducted. As shown in Figure 6C, humanised anti-CD26 mAb reduced the tumorigenicity of i.p. inoculated JMN (blue line, $P<0.0001$), while this anti-tumour effect was not observed in mice treated with the SSTR4 agonist L803087 alone (green or yellow lines). This *in vivo* anti-tumour effect was enhanced with the combined administration of humanised anti-CD26 mAb and SSTR4 agonist (red line in Figure 6C, $P<0.0001$). Taken together with results of the *in vitro* experiments presented in Figure 5C; Supplementary Figure S4A and B, our work illustrates the potency of the anti-tumour effect of the combination of humanised anti-CD26 mAb and the SSTR4 agonist on CD26-expressing MPM cells.

Coexpression of CD26 and SSTR4 is detected in surgical specimens of MPM patients. To explore the potential implications of SSTR4-mediated cytostatic effects in the clinical setting, we evaluated SSTR4 expression level in surgically resected human MPM tissues. Fifty consecutive surgically resected specimens from the primary sites were examined for membranous expression of SSTR4 and CD26. CD26 was highly expressed on epithelioid or biphasic type of MPM (panel b of Figure 7A and B), findings that were consistent with the results we showed previously (Aoe *et al*, 2012). In addition, SSTR4 was detected on epithelioid or biphasic type of MPM, predominantly coexpressed with membranous CD26 (panel c of Figure 7A and black bars of Figure 7B). These results suggest that selected MPM patients may be suitable candidates for a combined therapeutic approach with an anti-CD26 mAb and an SSTR4 agonist.

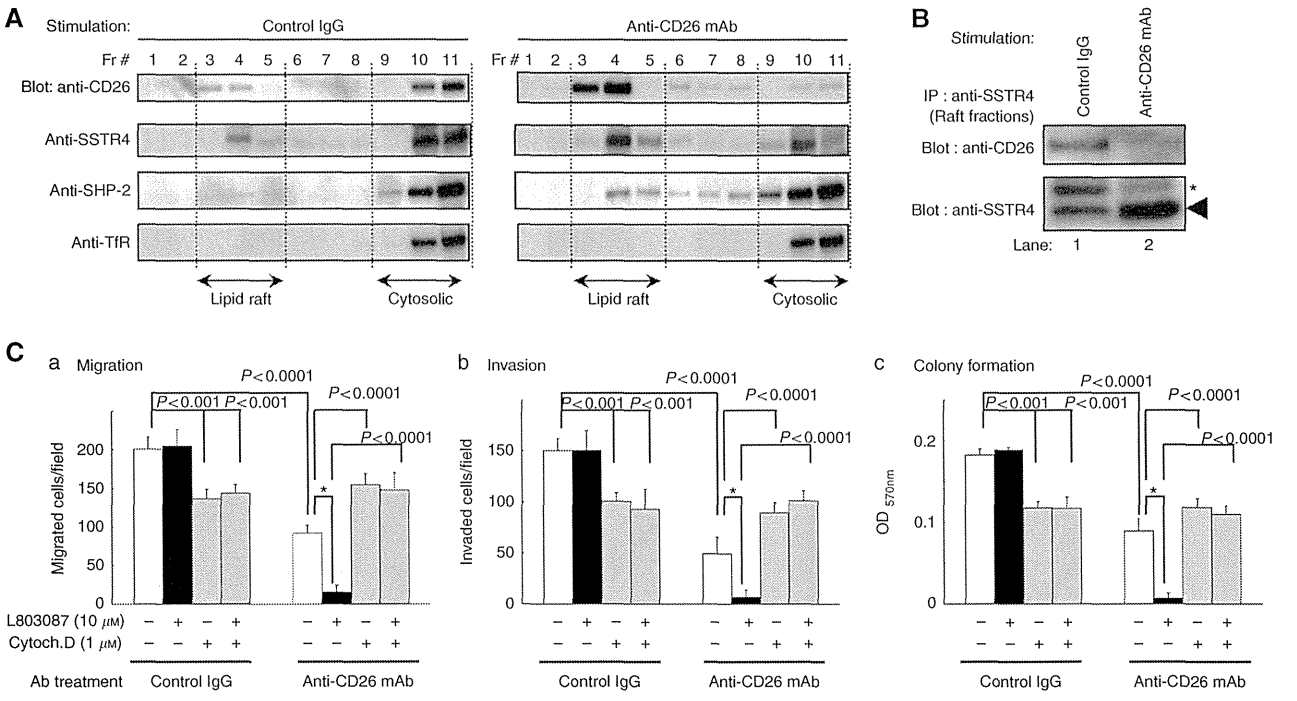

Figure 5. Humanised anti-CD26 mAb ligation promotes SSTR4 clustering with CD26 in lipid rafts and enhances SSTR4-mediated cytostatic effects. (**A**) MSTO-CD26WT cells were stimulated for 10 min with humanised anti-CD26 mAb alone (5.0 $\mu g\,ml^{-1}$), or with control human Ig (5.0 $\mu g\,ml^{-1}$) in the presence of anti-Fcγ (5.0 $\mu g\,ml^{-1}$). Lipid raft or cytosolic fractions were prepared by sucrose gradient ultracentrifugation. The distribution of CD26, SSTR4, SHP-2 and transferrin receptor (TfR) was determined by immunoblotting with specific antibodies. TfR is a representative of non-lipid raft proteins, and used as a quantity control indicating equal amounts in the experiments. Fraction number (Fr#) 3–5 or 9–11 contains lipid raft or cytosolic fractions, respectively. CD26, SSTR4 and SHP-2 molecules are recruited into the lipid raft fractions after anti-CD26 mAb treatment (upper three in the right panels). Similar results were obtained in three independent experiments. (**B**) MSTO-CD26WT cells were stimulated, and sucrose gradient ultracentrifugation was conducted by the same methods as in (**A**). Lipid raft fractions were pooled by collection of corresponding Fr#3–5. After being precleared with normal rabbit IgG, immunoprecipitation of lipid rafts with anti-SSTR4 rabbit pAb was performed, followed by resolution with SDS–PAGE, and immunoblotted with the indicated antibodies. After stimulation by anti-CD26 mAb, SSTR4 molecules were increased in lipid rafts (lane 2 of the lower panel), while the association of SSTR4 with CD26 molecules was decreased (lane 2 of the upper panel). Similar results were obtained in three independent experiments. * corresponds to the protein bands of immunoglobulin heavy chain, and arrow head, those of SSTR4. (**C**) MSTO-CD26WT cells adapted to the serum-reduced condition were incubated with 1 μM of cytochalasin D (Cytoch. D) or DMSO as a solvent control for 30 min, followed by cell migration (panel a), invasion (panel b) or colony formation assays (panel c) in the presence of the SSTR4 agonist L803087 (10 μM) or DMSO as a solvent control (mean ± s.e.m.; $n = 5$ experiments with triplicates). A significant decrease in anti-CD26 mAb-treated cell in control reagents was observed ($P < 0.0001$, white bars), and a more profound decrease was observed in the presence of L803087 (*, $P < 0.0001$). This reduction in the anti-CD26 mAb treatment group was restored in the presence of Cytoch. D ($P < 0.0001$). *P*-values are calculated by ANOVA with Tukey–Kramer *post hoc* test.

DISCUSSION

In this article, we show that CD26 is associated with SSTR4 in MPM cells, and this interaction inhibits SSTR4-mediated cytostatic effects. Moreover, we show using exogenous expression of deletion mutants that this molecular association needs the intracytoplasmic region of CD26 and the C-tail region of SSTR4. The present study also indicates that SSTR4-mediated cytostatic effects are transduced by SHP-2 PTP, and that this inhibitory effect is enhanced *via* lipid raft clustering of associated molecules following cross-linking of anti-CD26 mAb. Furthermore, using an *in vivo* xenograft model, we demonstrate that the anti-tumour effect of humanised anti-CD26 mAb is enhanced when combined with SSTR4 agonist treatment. Finally, we show that SSTR4 is highly coexpressed with CD26 on epithelioid or biphasic types of MPM tissues obtained from patients' surgical specimens.

We previously showed that anti-CD26 mAb inhibited growth of MPM cells and induced long-term survival of tumour-transplanted SCID mice (Inamoto *et al*, 2007). Recently, we showed that CD26 is preferentially expressed in MPM cells but not in normal mesothelial cells (Amatya *et al*, 2011), and suggested that membranous expression of CD26 is of potential importance in the treatment of MPM patients (Aoe *et al*, 2012). More recently, we showed that anti-CD26 mAbs induced the nuclear translocation of CD26 molecules to inhibit proliferation of MPM cells *via* suppression of *POLR2A* gene expression (Yamada *et al*, 2009, 2013). CD26 molecules were observed in the nucleus 30 min after anti-CD26 mAb treatment, peaking at 120 min and decreasing by 240 min. However, these findings did not provide an understanding of the earlier signalling events involved in the regulation of cell motility by CD26. Another regulatory mechanism for the malignant behaviour of CD26-expressing MPM cells involves the expression of CD9. We demonstrated that cells from certain CD26-positive MPM cell lines appeared to include the cancer stem cell characteristics for malignant mesothelioma in addition to $CD24^+$ $CD9^+$ cells (Ghani *et al*, 2011; Yamazaki *et al*, 2012), and that CD9 suppressed cell invasion and migration by inhibiting the formation of CD26–$\alpha5\beta1$ integrin complex with an associated decrease in phosphorylation of $\beta1$ integrin-related proteins such as focal adhesion kinase (FAK) and Crk-associated substrate lymphocyte type (Cas-L/HEF1/NEDD9) (Okamoto *et al*, 2014). Moreover, we showed that CD26 was associated with integrin-dependent adhesion of T-anaplastic large cell lymphoma Karpas

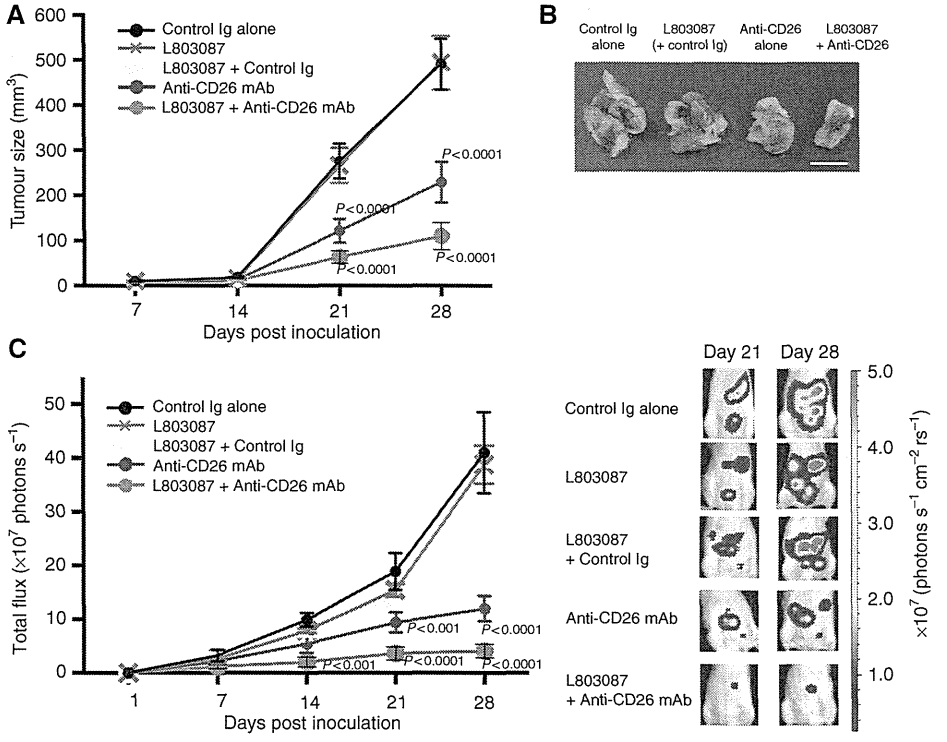

Figure 6. The inhibitory effect of combination of SSTR4 agonist and humanised anti-CD26 mAb on tumour growth in a murine xenograft model. (**A**) JMN cells (1×10^6) were inoculated s.c. into the left flank of mice. Mice were treated with i.p. injection of control IgG (10 μg per dose) alone, SSTR4 agonist L803087 (20 μM per dose) alone, L803087 (20 μM per dose) plus control IgG (10 μg per dose), humanised anti-CD26 mAb (10 μg per dose) alone or L803087 (20 μM per dose) plus humanised anti-CD26 mAb (10 μg per dose) on the seventh day post cancer cell inoculation, when the tumour mass became visible (5 mm in size). Each antibody or agonist was given three times per week. Each cohort was examined with $n = 20$. A significant decrease in the anti-CD26 mAb treatment cohort (blue line) was observed ($P < 0.0001$ *vs* control Ig, L803087 alone or L803087 plus control Ig cohort), and more profound decrease was observed in the L803087 plus anti-CD26 mAb treatment cohort (red line, $P < 0.0001$ *vs* control Ig, L803087 alone, L803087 plus control Ig or anti-CD26 mAb alone cohort). *P*-values are calculated by ANOVA with Tukey–Kramer *post hoc* test. (**B**) Representative macroscopic photo of resected specimens in an s.c. tumorigenicity model on the 28th day post first treatment. Scale bar indicates 1 cm. (**C**) After 1 day of i.p. injection of luciferase-expressing JMN cells (1×10^5), mice were treated with i.p. injection of control IgG (10 μg per dose), L803087 (20 μM per dose) plus control IgG (10 μg per dose), humanised anti-CD26 mAb (10 μg per dose) alone or L803087 (20 μM per dose) plus humanised anti-CD26 mAb (10 μg per dose). Each antibody or agonist was given three times per week. Tumour growth was measured by *in vivo* bioluminescence photometry, with imaging data of each cohort being indicated as total flux of photons per second (mean ± s.e.m.; $n = 20$). A significant decrease in anti-CD26 mAb treatment cohort (blue line) was observed ($P < 0.0001$ *vs* control Ig, L803087 alone or L803087 plus control Ig cohort), and a more profound decrease was observed in the L803087 plus anti-CD26 mAb treatment cohort (red line, $P < 0.0001$ *vs* control Ig, L803087 alone, L803087 plus control Ig or anti-CD26 mAb alone cohort). *P*-values are calculated by ANOVA with Tukey–Kramer *post hoc* test. Representative optical bioluminescence imaging of each cohort mice was shown with intensity of luminescence as heat maps in the right panels. The full colour version of this figure is available at *British Journal of Cancer* online.

299 to ECM by regulating p38-MAPK (mitogen-activated protein kinase)-dependent phosphorylation of β1 integrin (Sato *et al*, 2005). While these findings indicate that CD26 regulates ECM-associated tumour cell behaviour, the exact proximal molecular signalling events in tumour biology associated with the cytoplasmic region of CD26 remain to be elucidated, although those involved with the regulation of normal T-cell physiology have been well characterised (Ohnuma *et al*, 2008). In the present study, we demonstrate that the presence of the cytoplasmic, not the extracellular, region of CD26 resulted in enhanced MPM cell growth in *vivo* as well as *in vitro* migration, invasion and colony formation. In addition, we demonstrate that the cytoplasmic region of CD26 had a crucial role in MPM tumour biology through its linkage to SSTR4 and SHP-2 PTP in cell membrane lipid rafts, leading to cytostatic effects in MPM cells without direct association of ECM to CD26.

While SSTR subtypes have an important role in regulating tumour cell proliferation, SSTR4 is the least well-understood receptor among all the SSTR subtypes (Kumar, 2013). In the present study, we showed that SSTR4 was clearly expressed in MPM clinical specimens as well as various MPM cell lines, and that specific agonist for SSTR4 exhibited anti-tumour effects. Although these anti-tumour effects were blocked by coexpression of CD26, ligation of CD26 molecules by humanised anti-CD26 mAb induced lipid raft aggregation, leading to the activation of the cytostatic signalling molecule SHP-2 *via* clustering of SSTR4, which provides a platform for signalling events associated with multimerisation of SSTR4 molecules. Moreover, our observation that clustering of SSTR4 occurs in lipid raft is consistent with the findings that the C-terminal intracytoplasmic tail of SSTR4 and its oligomerisation are required for its cytostatic effects *via* SHP-2 recruitment in SSTR4-associated complex (Somvanshi *et al*, 2009). Although different pathways have been identified to regulate SST-induced inhibition of cell proliferation, according to the SSTR subtypes and experimental models, there is now an emerging consensus regarding the central role played by activation of PTPs in this process (Weckbecker *et al*, 2003; Florio, 2008). In fact, we showed that SHP-2 was required for SSTR4-mediated cytostatic effects in MPM cells, and that SHP-2 was clustered in lipid rafts along with the SSTR4 molecules that presumably disengaged from CD26.

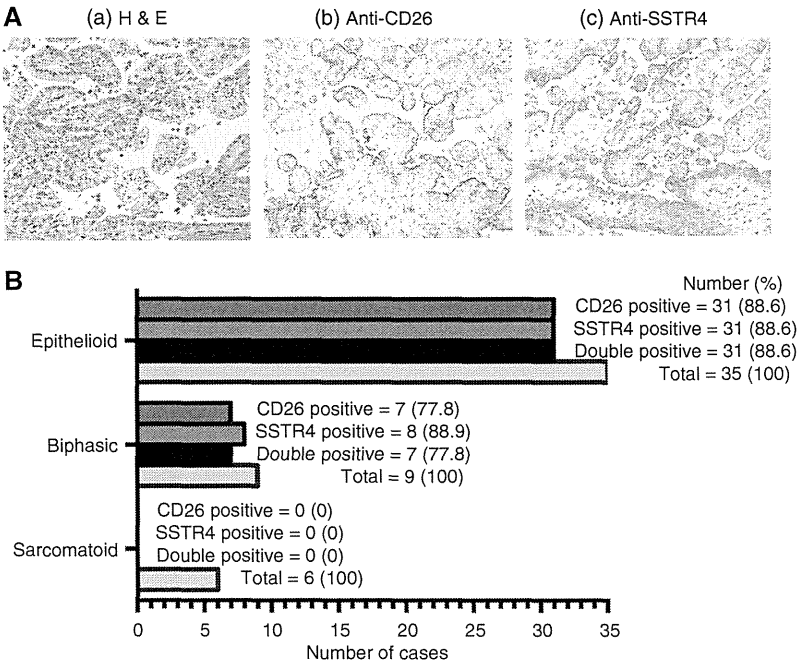

Figure 7. Coexpression of CD26 and SSTR4 in surgical specimens of MPM patients. (**A**) Representative serial sections of resected specimens of epithelioid type of malignant mesothelioma. Panel a, Haematoxylin and eosin (H&E) stain, panel b, anti-CD26 and panel c, anti-SSTR4 immunohistochemistry. Original magnification, x100. (**B**) CD26 and SSTR4 expression profile among 50 patient tissues. Fifty consecutive surgically resected specimens from the primary sites were examined for membranous expression of SSTR4 and CD26 by the same method as in (**A**). CD26 was highly expressed on epithelioid or biphasic type of MPM (purple bars), and SSTR4 was detected on epithelioid or biphasic type of MPM (red bars), predominantly coexpressed with membranous CD26 (black bars). The full colour version of this figure is available at *British Journal of Cancer* online.

Moreover, the SST-regulated PTPs control the activity of a number of downstream signalling molecules and, ultimately, induce an upregulation of cyclin-dependent kinase inhibitors (CDKIs), such as $p21^{cip1}$ and $p27^{kip1}$ (Reardon *et al*, 1997; Florio, 2008). These data support our previous findings that anti-CD26 mAb treatment induces upregulation of these CDKIs in T cells, renal carcinoma and MPM cells (Ohnuma *et al*, 2002; Inamoto *et al*, 2006, 2007).

As predicted by the mass-spectrometry analysis for proteins copurified with anti-CD26, we could not formally exclude the possibility that TRAK2, PEX1, actin or ribosomal proteins are involved in CD26-associated cell proliferation or mobility. It has been reported that TRAK2 and actin are cell membrane-associated proteins and that PEX1 or ribosomal proteins are abundantly located in peroxisomes or ribosomes (Tamura *et al*, 1998; Beck *et al*, 2002). In particular, actin or TRAK2 may interact with CD26 directly or indirectly to regulate the pathways involved in cell mobility (Beck *et al*, 2002; Buchan *et al*, 2002). Since our present effort aims to identify cell surface membrane proteins that can associate with the cytoplasmic region of CD26 in MPM cell lines, we focus our investigation on the membrane protein SSTR4 in the current study.

Although CD26/DPPIV is capable of cleaving N-terminal dipeptides with either L-proline or L-alanine at the penultimate position through its DPPIV activity (Ohnuma *et al*, 2008), the SSTR4 agonist used in the current study and the naturally occurring peptides SST-14 and SST-28 do not possess such amino-acid sequences (Bruns *et al*, 1994). Therefore, it is likely that the inhibition of SSTR4-mediated cytostatic effects observed in the present study is not due to cleavage of its agonists by CD26/DPPIV.

Meanwhile, data from the clinical samples obtained from patients with MPM revealed that SSTR4 is detected in almost all MPM tissues expressing membranous CD26. Taken together with the current *in vitro* observations, these results suggest that a novel therapeutic approach combining anti-CD26 mAb and an SSTR4 agonist may be of clinical benefit in selected patients with MPM, a notion that will be explored in future investigations. Likewise, the role of CD26 and SSTR4 coexpression as potential biomarkers and prognostic markers in MPM will be investigated in future studies.

In conclusion, we report that CD26 associates with SSTR4 in MPM cells, leading to high proliferative, migratory and invasive activities by CD26-expressing MPM cells. Humanised anti-CD26 mAb induces SSTR4 aggregation in lipid rafts and potentiates its cytostatic and anti-tumour effects. As SSTR4 and CD26 are found to coexpress in surgically resected specimens of human MPM, combination therapy using humanised anti-CD26 mAb and an SSTR4 agonist may provide clinical benefits in MPM.

ACKNOWLEDGEMENTS

We thank Ms. Aya Miwa and Ms. Haruna Otsuka for excellent assistance with laboratory work, and Drs. Yukio Takeshima, Vishwa Jeet Amatya and Kouki Inai for histopathological examination and classification of the clinical tissues. This study is supported by Grant-in-Aid of The Ministry of Education, Science, Sports (KO and CM) and Culture, Ministry of Health, Labour, and Welfare, Japan (CM).

CONFLICT OF INTEREST

CM is an inventor of the humanised CD26 mAb, YS110 (US Patent #7402698). Y's Therapeutics Co., Ltd owns this patent, and CM and NHD are founding members of this company.

AUTHOR CONTRIBUTIONS

JY, RH, TO, EK, HY and SI performed the experiments, interpreted the data and assisted with the paper, KO and CM designed the research, interpreted the data and wrote the paper, NHD interpreted the data, assisted with the paper, and proofread the manuscript, and KA, TK and TY provided the clinical data and samples, performed the experiments, analysed pathological results, interpreted the data and assisted with the paper.

REFERENCES

Amatya VJ, Takeshima Y, Kushitani K, Yamada T, Morimoto C, Inai K (2011) Overexpression of CD26/DPPIV in mesothelioma tissue and mesothelioma cell lines. *Oncol Rep* **26**: 1369–1375.

Aoe K, Amatya VJ, Fujimoto N, Ohnuma K, Hosono O, Hiraki A, Fujii M, Yamada T, Dang NH, Takeshima Y, Inai K, Kishimoto T, Morimoto C (2012) CD26 overexpression is associated with prolonged survival and enhanced chemosensitivity in malignant pleural mesothelioma. *Clin Cancer Res* **18**: 1447–1456.

Astoul P, Roca E, Galateau-Salle F, Scherpereel A (2012) Malignant pleural mesothelioma: from the bench to the bedside. *Respiration* **83**: 481–493.

Beck M, Brickley K, Wilkinson HL, Sharma S, Smith M, Chazot PL, Pollard S, Stephenson FA (2002) Identification, molecular cloning, and characterization of a novel $GABA_A$ receptor-associated protein, GRIF-1. *J Biol Chem* **277**: 30079–30090.

Brenner SL, Korn ED (1979) Substoichiometric concentrations of cytochalasin D inhibit actin polymerization. Additional evidence for an F-actin treadmill. *J Biol Chem* **254**: 9982–9985.

Britton M (2002) The epidemiology of mesothelioma. *Semin Oncol* **29**: 18–25.

Bruns C, Weckbecker G, Raulf F, Kaupmann K, Schoeffter P, Hoyer D, Lubbert H (1994) Molecular pharmacology of somatostatin-receptor subtypes. *Ann NY Acad Sci* **733**: 138–146.

Buchan AM, Lin CY, Choi J, Barber DL (2002) Somatostatin, acting at receptor subtype 1, inhibits Rho activity, the assembly of actin stress fibers, and cell migration. *J Biol Chem* **277**: 28431–28438.

Chien CH, Huang LH, Chou CY, Chen YS, Han YS, Chang GG, Liang PH, Chen X (2004) One site mutation disrupts dimer formation in human DPP-IV proteins. *J Biol Chem* **279**: 52338–52345.

Florio T (2008) Somatostatin/somatostatin receptor signalling: phosphotyrosine phosphatases. *Mol Cell Endocrinol* **286**: 40–48.

Froidevaux S, Eberle AN (2002) Somatostatin analogs and radiopeptides in cancer therapy. *Biopolymers* **66**: 161–183.

Ghani FI, Yamazaki H, Iwata S, Okamoto T, Aoe K, Okabe K, Mimura Y, Fujimoto N, Kishimoto T, Yamada T, Xu CW, Morimoto C (2011) Identification of cancer stem cell markers in human malignant mesothelioma cells. *Biochem Biophys Res Commun* **404**: 735–742.

Haas AR, Sterman DH (2013) Malignant pleural mesothelioma: update on treatment options with a focus on novel therapies. *Clin Chest Med* **34**: 99–111.

Havre PA, Abe M, Urasaki Y, Ohnuma K, Morimoto C, Dang NH (2008) The role of CD26/dipeptidyl peptidase IV in cancer. *Front Biosci* **13**: 1634–1645.

Ho L, Aytac U, Stephens LC, Ohnuma K, Mills GB, McKee KS, Neumann C, LaPushin R, Cabanillas F, Abbruzzese JL, Morimoto C, Dang NH (2001) *In vitro* and *in vivo* antitumor effect of the anti-CD26 monoclonal antibody 1F7 on human CD30+ anaplastic large cell T-cell lymphoma Karpas 299. *Clin Cancer Res* **7**: 2031–2040.

Inamoto T, Yamada T, Ohnuma K, Kina S, Takahashi N, Yamochi T, Inamoto S, Katsuoka Y, Hosono O, Tanaka H, Dang NH, Morimoto C (2007) Humanized anti-CD26 monoclonal antibody as a treatment for malignant mesothelioma tumors. *Clin Cancer Res* **13**: 4191–4200.

Inamoto T, Yamochi T, Ohnuma K, Iwata S, Kina S, Inamoto S, Tachibana M, Katsuoka Y, Dang NH, Morimoto C (2006) Anti-CD26 monoclonal antibody-mediated G1-S arrest of human renal clear cell carcinoma Caki-2 is associated with retinoblastoma substrate dephosphorylation, cyclin-dependent kinase 2 reduction, $p27^{kip1}$ enhancement, and disruption of binding to the extracellular matrix. *Clin Cancer Res* **12**: 3470–3477.

Ishii T, Ohnuma K, Murakami A, Takasawa N, Kobayashi S, Dang NH, Schlossman SF, Morimoto C (2001) CD26-mediated signaling for T cell activation occurs in lipid rafts through its association with CD45RO. *Proc Natl Acad Sci USA* **98**: 12138–12143.

Kumar U (2013) G-Protein coupled receptors dimerization: diversity in somatostatin receptors subtypes. *J Pharmacogenomics Pharmacoproteomics* **4**: 120–129.

Maguer-Satta V, Besancon R, Bachelard-Cascales E (2011) Concise review: neutral endopeptidase (CD10): a multifaceted environment actor in stem cells, physiological mechanisms, and cancer. *Stem Cells* **29**: 389–396.

Montironi R, Cheng L, Mazzucchelli R, Morichetti D, Stramazzotti D, Santinelli A, Moroncini G, Galosi AB, Muzzonigro G, Comeri G, Lovisolo J, Cosciani-Cunico S, Bono AV (2008) Immunohistochemical detection and localization of somatostatin receptor subtypes in prostate tissue from patients with bladder outlet obstruction. *Cell Oncol* **30**: 473–482.

Morimoto C, Schlossman SF (1998) The structure and function of CD26 in the T-cell immune response. *Immunol Rev* **161**: 55–70.

Myers R (2012) Asbestos-related pleural disease. *Curr Opin Pulm Med* **18**: 377–381.

Ogata S, Misumi Y, Ikehara Y (1989) Primary structure of rat liver dipeptidyl peptidase IV deduced from its cDNA and identification of the NH2-terminal signal sequence as the membrane-anchoring domain. *J Biol Chem* **264**: 3596–3601.

Ohnuma K, Dang NH, Morimoto C (2008) Revisiting an old acquaintance: CD26 and its molecular mechanisms in T cell function. *Trends Immunol* **29**: 295–301.

Ohnuma K, Ishii T, Iwata S, Hosono O, Kawasaki H, Uchiyama M, Tanaka H, Yamochi T, Dang NH, Morimoto C (2002) G1/S cell cycle arrest provoked in human T cells by antibody to CD26. *Immunology* **107**: 325–333.

Ohnuma K, Uchiyama M, Yamochi T, Nishibashi K, Hosono O, Takahashi N, Kina S, Tanaka H, Lin X, Dang NH, Morimoto C (2007) Caveolin-1 triggers T-cell activation via CD26 in association with CARMA1. *J Biol Chem* **282**: 10117–10131.

Ohnuma K, Yamochi T, Uchiyama M, Nishibashi K, Yoshikawa N, Shimizu N, Iwata S, Tanaka H, Dang NH, Morimoto C (2004) CD26 up-regulates expression of CD86 on antigen-presenting cells by means of caveolin-1. *Proc Natl Acad Sci USA* **101**: 14186–14191.

Okamoto T, Iwata S, Yamada H, Hatano R, Komiya E, Dang NH, Ohnuma K, Morimoto C (2014) CD9 negatively regulates CD26 expression and inhibits CD26-mediated enhancement of invasive potential of malignant mesothelioma cells. *PLoS One* **9**(1): e86671.

Patel YC (1999) Somatostatin and its receptor family. *Front Neuroendocrinol* **20**: 157–198.

Portela-Gomes GM, Stridsberg M, Grimelius L, Rorstad O, Janson ET (2007) Differential expression of the five somatostatin receptor subtypes in human benign and malignant insulinomas - predominance of receptor subtype 4. *Endocr Pathol* **18**: 79–85.

Reardon DB, Dent P, Wood SL, Kong T, Sturgill TW (1997) Activation *in vitro* of somatostatin receptor subtypes 2, 3, or 4 stimulates protein tyrosine phosphatase activity in membranes from transfected Ras-transformed NIH 3T3 cells: coexpression with catalytically inactive SHP-2 blocks responsiveness. *Mol Endocrinol* **11**: 1062–1069.

Reubi JC, Waser B, Schaer JC, Laissue JA (2001) Somatostatin receptor sst1-sst5 expression in normal and neoplastic human tissues using receptor autoradiography with subtype-selective ligands. *Eur J Nucl Med* **28**: 836–846.

Robinson BW, Lake RA (2005) Advances in malignant mesothelioma. *N Engl J Med* **353**: 1591–1603.

Rohrer SP (1998) Rapid identification of subtype-selective agonists of the somatostatin receptor through combinatorial chemistry. *Science* **282**: 737–740.

Sato T, Yamochi T, Yamochi T, Aytac U, Ohnuma K, McKee KS, Morimoto C, Dang NH (2005) CD26 regulates p38 mitogen-activated protein kinase-dependent phosphorylation of integrin β1, adhesion to extracellular matrix, and tumorigenicity of T-anaplastic large cell lymphoma Karpas 299. *Cancer Res* **65**: 6950–6956.

Shersher DD, Liptay MJ (2013) Multimodality treatment of pleural mesothelioma. *Surg Oncol Clin N Am* **22**: 345–355.

Somvanshi RK, Billova S, Kharmate G, Rajput PS, Kumar U (2009) C-tail mediated modulation of somatostatin receptor type-4 homo- and heterodimerizations and signaling. *Cell Signal* **21**: 1396–1414.

Takeshima Y, Inai K, Amatya VJ, Gemba K, Aoe K, Fujimoto N, Kato K, Kishimoto T (2009) Accuracy of pathological diagnosis of mesothelioma cases in Japan: clinicopathological analysis of 382 cases. *Lung Cancer* **66**: 191–197.

Tamura S, Okumoto K, Toyama R, Shimozawa N, Tsukamoto T, Suzuki Y, Osumi T, Kondo N, Fujiki Y (1998) Human PEX1 cloned by functional complementation on a CHO cell mutant is responsible for peroxisome-deficient Zellweger syndrome of complementation group I. *Proc Natl Acad Sci USA* **95**: 4350–4355.

Weckbecker G, Lewis I, Albert R, Schmid HA, Hoyer D, Bruns C (2003) Opportunities in somatostatin research: biological, chemical and therapeutic aspects. *Nat Rev Drug Discov* **2**: 999–1017.

Yamada K, Hayashi M, Du W, Ohnuma K, Sakamoto M, Morimoto C, Yamada T (2009) Localization of CD26/DPPIV in nucleus and its nuclear translocation enhanced by anti-CD26 monoclonal antibody with anti-tumor effect. *Cancer Cell Int* **9**: 17.

Yamada K, Hayashi M, Madokoro H, Nishida H, Du W, Ohnuma K, Sakamoto M, Morimoto C, Yamada T (2013) Nuclear localization of CD26 induced by a humanized monoclonal antibody inhibits tumor cell growth by modulating of POLR2A transcription. *PLoS One* **8**: e62304.

Yamazaki H, Naito M, Ghani FI, Dang NH, Iwata S, Morimoto C (2012) Characterization of cancer stem cell properties of CD24 and CD26-positive human malignant mesothelioma cells. *Biochem Biophys Res Commun* **419**: 529–536.

Yamochi T, Yamochi T, Aytac U, Sato T, Sato K, Ohnuma K, McKee KS, Morimoto C, Dang NH (2005) Regulation of p38 phosphorylation and topoisomerase IIα expression in the B-cell lymphoma line Jiyoye by CD26/dipeptidyl Peptidase IV is associated with enhanced *in vitro* and *in vivo* sensitivity to doxorubicin. *Cancer Res* **65**: 1973–1983.

Supplementary Information accompanies this paper on British Journal of Cancer website (http://www.nature.com/bjc)

CHEMBIOCHEM COMMUNICATIONS

ChemPubSoc Europe

DOI: 10.1002/cbic.201300762

Grassypeptolides as Natural Inhibitors of Dipeptidyl Peptidase 8 and T-Cell Activation

Jason C. Kwan,[a, b] Yanxia Liu,[a, c] Ranjala Ratnayake,[a, c] Ryo Hatano,[d] Akiko Kuribara,[d] Chiko Morimoto,[d] Kei Ohnuma,[d] Valerie J. Paul,[e] Tao Ye,[f] and Hendrik Luesch*[a, c]

Natural products made by marine cyanobacteria are often highly modified peptides and depsipeptides that have the potential to act as inhibitors for proteases. In the interests of finding new protease inhibition activity and selectivity, grassypeptolide A (**1**) was screened against a panel of proteases and found to inhibit DPP8 selectively over DPP4. Grassypeptolides were also found to inhibit IL-2 production and proliferation in activated T-cells, consistent with a putative role of DPP8 in the immune system. These effects were also observed in Jurkat cells, and DPP activity in Jurkat cell cytosol was shown to be inhibited by grassypeptolides. In silico docking suggests two possible binding modes of grassypeptolides—at the active site of DPP8 and at one of the entrances to the internal cavity. Collectively these results suggest that grassypeptolides might be useful tool compounds in the study of DPP8 function.

Although originally thought to perform only degradative and catabolic functions, proteases are now recognized to be involved in regulation of diverse biological processes, from blood coagulation to immune function.[1] Because of this, they are potentially attractive drug targets in many therapeutic areas.[2] However, because of the ubiquitous nature of protease regulation, nonspecific inhibitors could suffer from serious off-target effects. For example, the clinical development of matrix metalloprotease (MMP) inhibitors for treatment of cancer largely failed due to nonspecific inhibition.[2] Several MMPs had not been discovered at the time of the development of these agents, and there was an inadequate understanding of the importance of MMPs in prosurvival pathways.[2] Molecular tool compounds that have differing selectivities for different members of a protease family might help delineate the functions of cryptic members, and this is especially needed for enzymes of unknown function that are related to drug targets. Natural products are a potential source of such tool compounds. As products of evolution, they often exhibit bioactivity against specific protein targets, and in fact account for the majority of pharmacophores of drugs in use today.[3] Importantly, natural products generally have highly complex and densely functionalized structures that differ significantly from the results of human rational drug design.

In our own efforts, we have identified several natural products that inhibit proteases. Free-living marine cyanobacteria have proved to be a prolific source of modified peptides, which are presumably produced as a form of chemical defense.[4] We have found two groups of natural protease inhibitors: lyngbyastatins 8–10[5] and symplostatin 5,[6] which potently inhibit the serine protease elastase, and the grassystatins,[7] which preferentially inhibit the aspartic protease cathepsin E. We have also designed synthetic analogues of tasiamide B[8,9] that inhibit another aspartic protease—BACE1—that is implicated in Alzheimer's disease.

Another group of compounds that we have isolated are grassypeptolides A–C (**1**–**3**), bis-thiazoline-containing cyclic depsipeptides from samples of *Lyngbya confervoides*.[10,11] Previously, **1**–**3** were found to be cytotoxic to a variety of transformed human cancer cell lines, with **3** being the most potent.

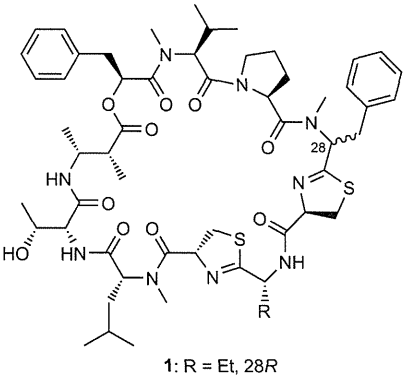

1: R = Et, 28*R*
2: R = Me, 28*R*
3: R = Et, 28*S*

[a] *Dr. J. C. Kwan, Dr. Y. Liu, Dr. R. Ratnayake, Prof. Dr. H. Luesch*
Department of Medicinal Chemistry
College of Pharmacy, University of Florida
1345 Center Drive, Gainesville FL 32610 (USA)
E-mail: luesch@cop.ufl.edu

[b] *Dr. J. C. Kwan*
Current address: Pharmaceutical Sciences Division
School of Pharmacy, University of Wisconsin-Madison
777 Highland Ave, Madison WI 53705 (USA)

[c] *Dr. Y. Liu, Dr. R. Ratnayake, Prof. Dr. H. Luesch*
Center for Natural Products, Drug Discovery and Development (CNPD3)
University of Florida
1345 Center Drive, Gainesville FL 32610 (USA)

[d] *R. Hatano, A. Kuribara, Prof. Dr. C. Morimoto, Dr. K. Ohnuma*
Division of Clinical Immunology, Advanced Clinical Research Centre
Institute of Medical Science, University of Tokyo
4-6-1, Shirokanedai, Minato-ku, Tokyo 1088639 (Japan)

[e] *Dr. V. J. Paul*
Smithsonian Marine Station
701 Seaway Drive, Fort Pierce FL 34949 (USA)

[f] *Prof. Dr. T. Ye*
Department of Applied Biology & Chemical Technology
The Hong Kong Polytechnic University
Hung Hom, Kowloon, Hong Kong (P. R. China)

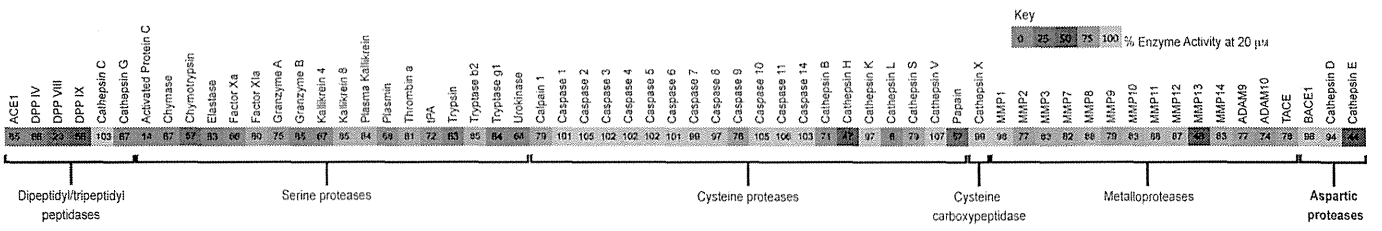

Figure 1. Protease panel treated with grassypeptolide A (**1**, 20 μM). Values represent % residual enzyme activity relative to solvent control and are additionally represented by a continuous color scale (0% red, 100% green).

Our total synthesis of grassypeptolide A (**1**) confirmed the structure.[12] Synthetic material was used to demonstrate that **1** downregulates cyclin D and upregulates p27 and p21 to modulate cell cycle distribution, and that the compound increases PARP cleavage and decreases BCL-2 and BCL-xL expression, correlating with the proapoptotic activity of **1**.[12] Additional grassypeptolides were discovered by other groups;[13,14] all show some degree of toxicity, and analogues with 28*S* configuration, such as **3**, show the greatest potency.

Prompted by findings for similar cyclic peptides,[15,16] we investigated the metal binding of **1** and **3** and found that they bind to Cu^{2+} and Zn^{2+} ions.[11] Both of these metals are known to play crucial roles in the mechanism of certain enzymes: the MMPs and CuZn-superoxide dismutase, for example. In this work we therefore decided to screen grassypeptolide A (**1**, the most abundant natural product of the series) against a representative panel of proteases (Figure 1). However, except for a weak effect on MMP13, we did not see inhibition of any metalloprotease in the panel. Instead, the strongest hits were the cysteine protease cathepsin L (Cat L), the serine protease activated protein C (APC) and the dipeptidyl peptidase (DPP) DPP8, which were inhibited to 6, 14 and 23% residual activity, respectively, relative to solvent control at a screening concentration of 20 μM.

We investigated the three hits further by determining the IC_{50} values of inhibition for grassypeptolides A–C (**1**–**3**, see Table 1). For all compounds, the IC_{50} values fell in the order DPP8 < Cat L < APC. Importantly, all three compounds showed selectivity for DPP8 over DPP4, ranging from 9.9-fold (**2**) to 38.2-fold (**3**). The selectivity is less than that of some isoindoline N-capped amino-acid-derived DPP8/9 inhibitors.[17–19] The most potent of these synthetic inhibitors has an IC_{50} of 8.8 nM against DPP8 and a selectivity of over 11 000 for DPP8 versus DPP4,[19] but the grassypeptolides represent a new structural class of DPP inhibitors. We previously found **3** to be more cytotoxic than either **1** or **2**. Because **3** has a similar inhibitory potency against DPP8 relative to **1** and **2**, this activity is probably not responsible for toxicity in the tested cancer cell lines.

Table 1. IC_{50} values of grassypeptolides against cathepsin L, dipeptidyl peptidases and activated protein C.

	IC_{50} [μM]			
Compound	Cat L	DPP4	DPP8	APC
grassypeptolide A (**1**)	14.0	347	11.5	79.0
grassypeptolide B (**2**)	21.3	164	16.6	66.6
grassypeptolide C (**3**)	20.4	245	6.41	62.0
control[a]	0.000238	0.155	1.45	1.40

[a] For cathepsin L, the positive control inhibitor was E64, for DPP4 and DPP8 the control inhibitor was P32/98, and for APC the positive control was gabexate mesylate.

DPP8 is closely related to DPP4, a validated target in the treatment of type 2 diabetes.[20] A handful of DPP4 inhibitors are currently marketed for this indication, and several more are in development.[20] Inhibition of DPP4 leads to an increase in one of its substrates, GLP-1, which in turn stimulates insulin production and inhibits glucagon release, thus lowering blood glucose.[20] Both DPP8 and DPP9 are widely expressed in different tissues,[21] but the functions of these two enzymes have not been delineated. Some evidence points to roles in the immune system for both DPP8 and DPP9. Both enzymes, for example, are upregulated in a rat model of asthma, whereas expression levels of DPP4 are unchanged.[22] DPP9 has also been implicated in the general turnover of proline-containing peptides, potentially exerting control over which cytosolic peptides are presented as antigens by MHC class I complexes.[23] The first known natural substrate of DPP9 was the antigenic peptide $RU1_{34-42}$—in this case action of DPP9 reduces presentation of the mature epitope.[23] There remains little direct evidence of DPP8/9 involvement in immune system function, and recent work implicates DPP8/9 in other processes, such as epidermal growth factor signaling[24] and energy homeostasis.[25] Additional selective inhibitors that could be used as tool compounds might thus be useful for further study of these enzymes.

Because DPP8 has been implicated in immune system functions, we investigated the effect of grassypeptolide A (**1**) on the activation of T-cells by exogenous anti-CD3 and anti-CD28. These antibodies simulate co-stimulation of the T-cell receptor (which includes CD3 as a subunit) and CD28, leading to T-cell activation. We found that **1** was able to reduce IL-2 production, one of the hallmarks of T-cell activation (see Figure 2A). We also found a reduction in the stimulated T-cell proliferation seen in response to anti-CD3/CD28 (see Figure 2B). Previously, similar results were also observed for human T-cells in vitro with another selective DPP8/9 inhibitor;[26] this potentially implicates DPP8 or DPP9 in this effect.

We went on to corroborate this finding by investigating the effect of grassypeptolides B (**2**) and C (**3**) in the transformed Jurkat cell line,[27] which has T-cell characteristics and produces IL-2 upon appropriate stimulation. We found that both compounds were able to reduce the production of IL-2 in response

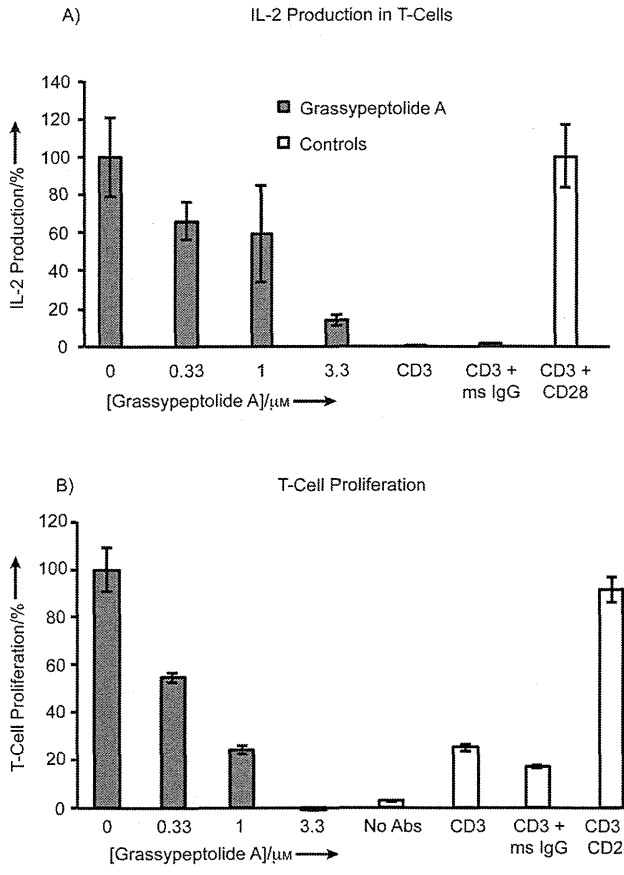

Figure 2. A) Effect of grassypeptolide A (**1**) on IL-2 production by T-cells in response to anti-CD3/CD28. B) Effect of grassypeptolide A (**1**) on T-cell proliferation in response to anti-CD3/CD28.

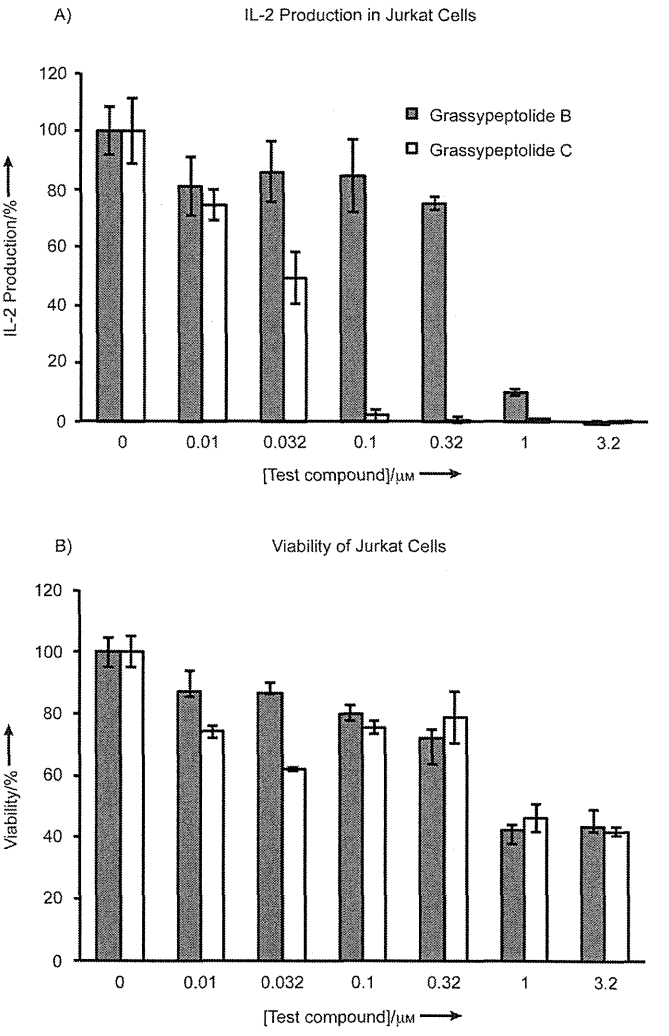

Figure 3. A) Effect of grassypeptolides B (**2**) and C (**3**) on IL-2 production by Jurkat cells in response to PMA and PHA. B) Effect of grassypeptolides B (**2**) and C (**3**) on viability in Jurkat cells stimulated with PMA and PHA.

to dual stimulation with phorbol 12-myristate 13-acetate (PMA) and phytohemagglutinin (PHA, see Figure 3A).[28] In this cell line we observed a less dramatic effect on proliferation (Figure 3B); this indicates that reduction in IL-2 production is not a simple function of cell number.

We sought to determine whether DPP activity was indeed being compromised in Jurkat cells by treatment with **1**. We therefore prepared subcellular fractions of cells corresponding to cell membranes and cytosol, and tested the effect of **1** on the cleavage of a DPP substrate by enzymes in these fractions. DPP4 is a membrane-bound protein, whereas DPP8 and DPP9 are found in the cytosol.[29] Our results, shown in Figure 4, are consistent with selective inhibition of DPP8/9 over DPP4 because we found that **1** inhibited DPP-like activity to a greater extent in the cytosol fraction than in the membrane fraction. Concurrently, the nonselective control inhibitor P32/98 showed similar potency in both cell fractions. The potency of **1** in this assay is much less than exhibited in live Jurkat cells (Figure 3). This might reflect additional uninhibited enzymes carrying out DPP-like activity in crude lysates or inefficient inhibition of cleavage with an artificial substrate (vide infra), or it might indicate that the reduction of IL-2 production could be mediated by another mechanism.

Because **1** is a new structural class of DPP inhibitor, we sought to explain its inhibitory activity on DPP8 by carrying out in silico molecular docking of **1** into a previously reported homology model of DPP8.[30] Like related enzyme structures, the DPP8 homology model has a large internal cavity where the active site resides. This cavity is accessible from two openings—the main opening, which is proximal to the catalytic triad (Ser739, His849, Asp817), and the narrower opening formed by the eight-bladed β-propeller domain at the opposite end of the protein. When we used the entire internal surface of DPP8 as the search space for molecular docking, it was found that **1** docked to two distinct regions (Figure 5). Interestingly, docking to the inside surface of the propeller opening gave lower calculated binding energies than docking to the other side close to the catalytic triad (−10.5 vs. −9.5 kcal mol^{-1}, respectively).

The docking pose of **1** close to the active site (pose 1) does not bring the compound into contact with the proline binding site, nor with the P2 site previously proposed to be important for other classes of inhibitors.[31] This pose is possibly stabilized by π–π interactions between the *N*-Me-Phe unit of **1** and the P1 pocket of the hydrolase domain, containing many aromatic

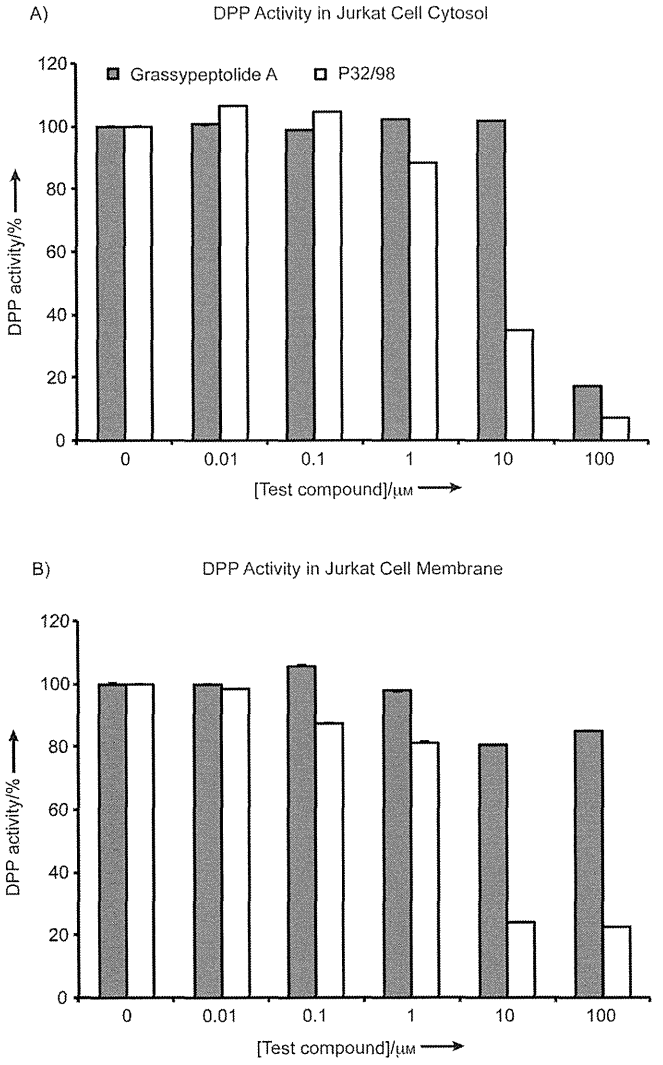

Figure 4. Effect of grassypeptolide A (**1**) on DPP activity in A) Jurkat cell cytosol, and B) Jurkat cell membrane fractions.

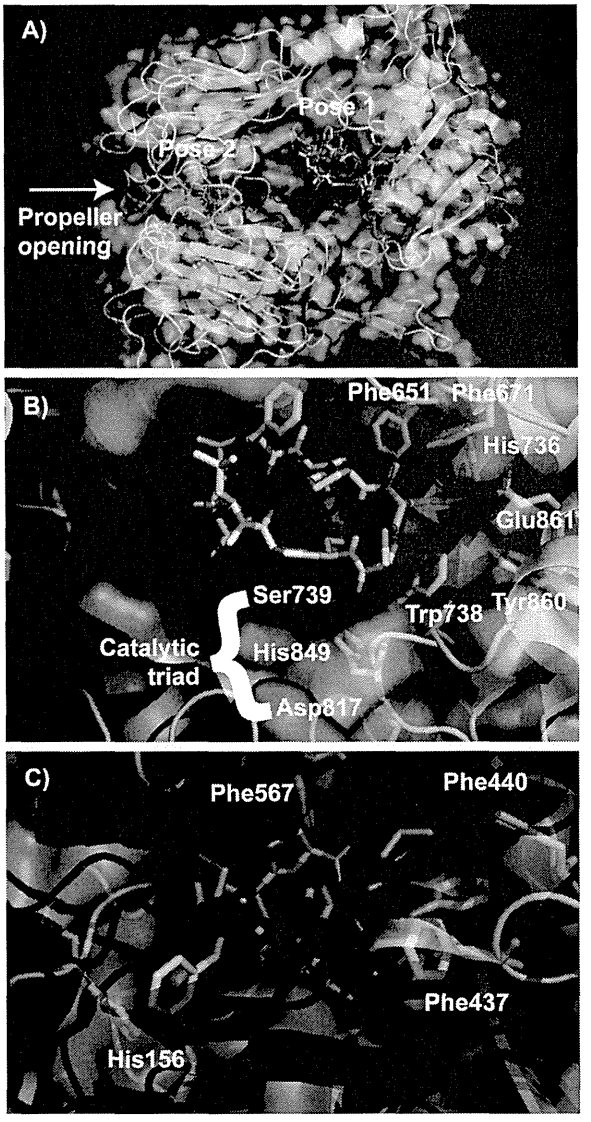

Figure 5. Two docked poses of grassypeptolide A (**1**) generated by in silico molecular docking into a homology model of DPP8. A) Overview of the two identified binding sites. B) Close-up of pose 1 (close to active site), showing the catalytic triad and aromatic residues close to the *N*-Me-Phe unit of **1**. C) Close-up of pose 2 (inside surface of propeller opening), showing aromatic residues close to the phenyl rings or other π bonds of **1**.

residues (Phe651, Phe671, His736, Trp738 and Tyr860, also known as the T-stacking conserved aromatic motif,[30] see Figure 5). Interestingly, DPP4 possesses an extra aromatic residue in this pocket—Tyr752 (Glu861 in the DPP8 homology model, see Figure S1 in the Supporting Information). If pose 1 is placed in an aligned X-ray structure of DPP4 (PDB ID: 2BGR),[32] it can be seen that a steric clash would occur between the *N*-Me-Phe and Tyr752. Compound **1** does dock into DPP4 at this site, but the *N*-Me-Phe is not bound so deeply in the aromatic pocket (see Figure S1). Potentially, deeper binding of the *N*-Me-Phe side chain in the pocket could perturb the relative positions of the β-sheet and α-helix that are attached to the active-site residues Ser739 and His849, respectively.

Likewise, at the propeller opening site (pose 2), there are several aromatic residues that could engage in π–π interactions to **1** (His156, Phe437, Phe440, Phe567, see Figure 5). In DPP4 these are replaced by Ser106, Glu361, His363 and Lys463, respectively, and so **1** docks into DPP4 at this site with a different orientation, in which there is a likely edge-to-face π–π interaction with Trp215 (see Figure S1). Binding at this site would effectively block the propeller opening in both DPP4 and DPP8, and therefore might disproportionately affect cleavage of substrates that use this entrance. Because the substrate used in our enzymatic inhibition experiments (H-GP-AMC) is fairly small, inhibition by blocking the propeller opening might not have been detected. In light of the docking results, the mode of inhibition might simply be steric hindrance of the substrate around the active site, along with prevention of its entrance through the propeller opening. Both of these might be more effective inhibition strategies against larger substrates, and this could potentially explain the fairly high IC_{50} values when measured with a small substrate (H-GP-AMC), relative to the effect on T-cells. Some candidate substrates for

DPP8 have been identified through proteomics,[25] and all of them are proteins containing more than 200 amino acids. These larger substrates might require the propeller opening, or they might be less able than a smaller substrate to displace **1** from the active site.

We have shown that the grassypeptolides inhibit DPP8, and molecular docking suggests that **1** might bind to the inner cavity of the enzyme at two distinct sites. The compound thus might prove to be a valuable tool for studying the relative importance of the propeller opening for different substrates when they are identified.

Experimental Section

Isolation of grassypeptolides: The grassypeptolides were isolated from samples of *L. confervoides* as previously described.[11] After natural sources of grassypeptolide A were exhausted, material obtained through total synthesis[12] was used.

Protease inhibition screen: The initial protease screen was carried out as previously described,[7] by Reaction Biology Corp. (Malvern, PA, with 20 μM **1**). Follow-up experiments to determine the IC_{50} values of **1**–**3** used the same conditions as for the screen but with a range of concentrations for the test compounds, each in duplicate.

T-cell IL-2 and proliferation assay: Human CD3+ T-cells were purified from peripheral blood mononuclear cells from a healthy adult volunteer, with use of a MACS Pan T-cell Isolation Kit (Miltenyi Biotech). A 96-well plate was coated with murine anti-CD3 (OKT3, 0.5 $\mu g\,mL^{-1}$) and anti-CD28 (4B10, 5 $\mu g\,mL^{-1}$) as previously described.[33] T-cells were added to the precoated plate (1×10^5 cells/well), and incubated in serum-free AIM-V medium in the presence of different concentrations of grassypeptolide A (**1**, added as a solution in DMSO) for 48 h. Concentrations of IL-2 in the supernatants were then quantified by sandwich ELISA. To quantify proliferation, cells were grown under the same conditions for 48 h, after which time MTT dye was added to wells in order to measure relative cell number.

Jurkat IL-2 and viability assay: Jurkat cells were grown in 96-well plates (100000 cells/well), in RPMI-1640 medium in the presence of PMA (80 nM, Sigma–Aldrich, added as a solution in DMSO), PHA (10 $\mu g\,mL^{-1}$, Sigma–Aldrich, added as a solution in PBS), and varying concentrations of **2** or **3** (added as 100-fold freshly prepared stock solutions in EtOH), by the procedure of Fischer et al.[28] The DMSO content of the culture wells was kept below 0.25% because it was found to be toxic to Jurkat cells at higher levels. After 24 h incubation at 37 °C in a humidified atmosphere containing CO_2 (5%), the IL-2 content of the supernatants was quantified with the aid of a hIL-2 alphaLISA kit and an EnVision detector (PerkinElmer). To quantify viability, cells were grown under the same conditions and then developed with MTT dye by the manufacturer's protocol (Promega).

Jurkat cell endogenous DPP activity assay: Jurkat cells were grown and subjected to subcellular fractionation as described by Rockstroh et al.[34] Various concentrations of compound or solvent control, subcellular fractions and substrate were preincubated for 10 min at 37 °C, after which the absorbance at 405 nm was monitored for 5 min with a microplate reader.[35] The slope was used to quantify enzyme activity. The amount of protein in the cytosolic/membrane fraction used for each reaction was 500 μg, obtained from 5×10^6 cells. DPP8/9 and DPP4 activity were determined separately in cytosolic and membrane fractions with the substrate Gly-Pro-pNA [0.5 mM in Tris buffer (pH 8.3, 0.05 M) containing EDTA (10 mM) and aprotinin (14 $\mu g\,mL^{-1}$)]. Both Gly-Pro-pNA and P32/98 (positive control inhibitor) were obtained from Enzo (Farmingdale, NY).

Molecular docking: A previously determined crystal structure of compound **1**[10] was docked into DPP4 and DPP8 by use of Autodock Vina 1.1.1,[36] with an exhaustiveness value of 100 and with a search box encompassing the entire interior of the appropriate protein. A previously published homology model of DPP8 was used[30] because no crystal structure is available. The crystal structure 2BGR was used for docking to DPP4[32] because this structure was the basis of the DPP8 homology model. The two proteins were aligned to each other in PyMOL (Schrödinger, LLC) prior to docking in order to aid comparison between the docking poses of each. Each docking run produced 100 binding modes, which were examined in ascending order of calculated binding energy. The binding poses shown in Figure 5 are the lowest-binding-energy structures of the two binding sites found in the total set of binding modes.

Acknowledgements

This research was supported in part by the National Institutes of Health, NIGMS grant P41GM086210 and NCI grant R01CA172310. We wish to thank Christian Rummey for kindly providing the homology model of DPP8. We would also like to thank Nam Dang for helpful discussions. This is contribution 940 from the Smithsonian Marine Station at Fort Pierce.

Keywords: dipeptidyl peptidases · grassypeptolides · immunochemistry · natural products · protease inhibition

[1] C. López-Otín, J. S. Bond, *J. Biol. Chem.* **2008**, *283*, 30433–30437.
[2] B. Turk, *Nat. Rev. Drug Discovery* **2006**, *5*, 785–799.
[3] D. J. Newman, G. M. Cragg, *J. Nat. Prod.* **2012**, *75*, 311–335.
[4] L. T. Tan, *Phytochemistry* **2007**, *68*, 954–979.
[5] J. C. Kwan, K. Taori, V. J. Paul, H. Luesch, *Mar. Drugs* **2009**, *7*, 528–538.
[6] L. A. Salvador, K. Taori, J. S. Biggs, J. Jakoncic, D. A. Ostrov, V. J. Paul, H. Luesch, *J. Med. Chem.* **2013**, *56*, 1276–1290.
[7] J. C. Kwan, E. A. Eksioglu, C. Liu, V. J. Paul, H. Luesch, *J. Med. Chem.* **2009**, *52*, 5732–5747.
[8] P. G. Williams, W. Y. Yoshida, R. E. Moore, V. J. Paul, *J. Nat. Prod.* **2003**, *66*, 1006–1009.
[9] Y. Liu, W. Zhang, L. Li, L. A. Salvador, T. Chen, W. Chen, K. M. Felsenstein, T. B. Ladd, A. R. Price, T. E. Golde, J. He, Y. Xu, Y. Li, H. Luesch, *J. Med. Chem.* **2012**, *55*, 10749–10765.
[10] J. C. Kwan, J. R. Rocca, K. A. Abboud, V. J. Paul, H. Luesch, *Org. Lett.* **2008**, *10*, 789–792.
[11] J. C. Kwan, R. Ratnayake, K. A. Abboud, V. J. Paul, H. Luesch, *J. Org. Chem.* **2010**, *75*, 8012–8023.
[12] H. Liu, Y. Liu, Z. Wang, X. Xing, A. R. Maguire, H. Luesch, H. Zhang, Z. Xu, T. Ye, *Chem. Eur. J.* **2013**, *19*, 6774–6784.
[13] C. C. Thornburg, M. Thimmaiah, L. A. Shaala, A. M. Hau, J. M. Malmo, J. E. Ishmael, D. T. A. Youssef, K. L. McPhail, *J. Nat. Prod.* **2011**, *74*, 1677–1685.
[14] W. L. Popplewell, R. Ratnayake, J. A. Wilson, J. A. Beutler, N. H. Colburn, C. J. Henrich, J. B. McMahon, T. C. McKee, *J. Nat. Prod.* **2011**, *74*, 1686–1691.
[15] A. Bertram, G. Pattenden, *Nat. Prod. Rep.* **2007**, *24*, 18–30.
[16] W. E. Houssen, M. Jaspars, *ChemBioChem* **2010**, *11*, 1803–1815.
[17] P. Van der Veken, A. Soroka, I. Brandt, Y.-S. Chen, M.-B. Maes, A.-M. Lambeir, X. Chen, A. Haemers, S. Scharpé, K. Augustyns, I. De Meester, *J. Med. Chem.* **2007**, *50*, 5568–5570.

[18] S. Van Goethem, P. Van der Veken, V. Dubois, A. Soroka, A.-M. Lambeir, X. Chen, A. Haemers, S. Scharpé, I. De Meester, K. Augustyns, *Bioorg. Med. Chem. Lett.* **2008**, *18*, 4159–4162.
[19] S. Van Goethem, V. Matheeussen, J. Joossens, A.-M. Lambeir, X. Chen, I. De Meester, A. Haemers, K. Augustyns, P. Van der Veken, *J. Med. Chem.* **2011**, *54*, 5737–5746.
[20] C. F. Deacon, *Diabetes Obes. Metab.* **2011**, *13*, 7–18.
[21] D. M. T. Yu, K. Ajami, M. G. Gall, J. Park, C. S. Lee, K. A. Evans, E. A. McLaughlin, M. R. Pitman, C. A. Abbott, G. W. McCaughan, M. D. Gorrell, *J. Histochem. Cytochem.* **2009**, *57*, 1025–1040.
[22] J. Schade, M. Stephan, A. Schmiedl, L. Wagner, A. J. Niestroj, H.-U. Demuth, N. Frerker, C. Klemann, K. A. Raber, R. Pabst, S. von Hörsten, *J. Histochem. Cytochem.* **2008**, *56*, 147–155.
[23] R. Geiss-Friedlander, N. Parmentier, U. Möller, H. Urlaub, B. J. Van den Eynde, F. Melchior, *J. Biol. Chem.* **2009**, *284*, 27211–27219.
[24] T.-W. Yao, W.-S. Kim, D. M. T. Yu, G. Sharbeen, G. W. McCaughan, K.-Y. Choi, P. Xia, M. D. Gorrell, *Mol. Cancer Res.* **2011**, *9*, 948–959.
[25] C. H. Wilson, D. Indarto, A. Doucet, L. D. Pogson, M. R. Pitman, K. McNicholas, R. I. Menz, C. M. Overall, C. A. Abbott, *J. Biol. Chem.* **2013**, *288*, 13936–13949.
[26] G. R. Lankas, B. Leiting, R. S. Roy, G. J. Eiermann, M. G. Beconi, T. Biftu, C.-C. Chan, S. Edmondson, W. P. Feeney, H. He, D. E. Ippolito, D. Kim, K. A. Lyons, H. O. Ok, R. A. Patel, A. N. Petrov, K. A. Pryor, X. Qian, L. Reigle, A. Woods, et al., *Diabetes* **2005**, *54*, 2988–2994.
[27] U. Schneider, H.-U. Schwenk, G. Bornkamm, *Int. J. Cancer* **1977**, *19*, 621–626.
[28] B. S. Fischer, D. Qin, K. Kim, T. V. McDonald, *J. Pharmacol. Exp. Ther.* **2001**, *299*, 238–246.
[29] H.-K. Tang, K.-C. Chen, G.-G. Liou, S.-C. Cheng, C.-H. Chien, H.-Y. Tang, L.-H. Huang, H.-P. Chang, C.-Y. Chou, X. Chen, *FEBS Lett.* **2011**, *585*, 3409–3414.
[30] C. Rummey, G. Metz, *Proteins Struct. Funct. Bioinf.* **2007**, *66*, 160–171.
[31] S. Nordhoff, S. Cerezo-Gálvez, A. Feurer, O. Hill, V. G. Matassa, G. Metz, C. Rummey, M. Thiemann, P. J. Edwards, *Bioorg. Med. Chem. Lett.* **2006**, *16*, 1744–1748.
[32] W. A. Weihofen, J. Liu, W. Reutter, W. Saenger, H. Fan, *J. Biol. Chem.* **2005**, *280*, 14911–14917.
[33] R.-P. Dong, Y. Umezawa, H. Ikushima, Y. Munakata, S. F. Schlossman, C. Morimoto, *J. Clin. Immunol.* **1997**, *17*, 247–252.
[34] M. Rockstroh, S. A. Müller, C. Jende, A. Kerzhner, M. von Bergen, J. M. Tomm, *J. Integr. OMICS* **2011**, *1*, 135–143.
[35] M.-B. Maes, V. Dubois, I. Brandt, A.-M. Lambeir, P. Van der Veken, K. Augustyns, J. D. Cheng, X. Chen, S. Scharpé, I. De Meester, *J. Leukocyte Biol.* **2007**, *81*, 1252–1257.
[36] O. Trott, A. J. Olson, *J. Comput. Chem.* **2010**, *31*, 455–461.

Received: December 4, 2013
Published online on March 3, 2014

Hatano et al. Diagnostic Pathology 2014, 9:30
http://www.diagnosticpathology.org/content/9/1/30

DIAGNOSTIC PATHOLOGY

RESEARCH Open Access

Establishment of monoclonal anti-human CD26 antibodies suitable for immunostaining of formalin-fixed tissue

Ryo Hatano[1], Taketo Yamada[2], Shuji Matsuoka[3], Satoshi Iwata[1], Hiroto Yamazaki[1], Eriko Komiya[1], Toshihiro Okamoto[1], Nam H Dang[4], Kei Ohnuma[1] and Chikao Morimoto[1*]

Abstract

Background: A T cell costimulatory molecule with dipeptidyl peptidase IV (DPPIV) activity in its extracellular region, CD26 is a multifunctional molecule associated with various proteins such as adenosine deaminase, caveolin-1, CXCR4, collagen, and fibronectin, while playing an important role in the regulation of inflammatory responses and tumor biology. We have focused on CD26 as a novel therapeutic target for various tumors and immune disorders, and have developed a humanized anti-CD26 monoclonal antibody (mAb), YS110, which is currently being evaluated in a phase I clinical trial for patients with CD26-expressing tumors, including malignant mesothelioma. Since detection of tumor CD26 expression is required for determining potential eligibility for YS110 therapy, the development of anti-human CD26 mAb that can clearly and reliably detect the denatured CD26 molecule in the formalin-fixed paraffin-embedded tissues is critical.

Methods: To develop novel anti-CD26 mAbs capable of binding to the denatured CD26, we immunized mice with CD26 protein denatured in urea buffer. After the fusion of splenocytes and myeloma cells, the mAbs were screened for specific reactivity with human CD26 by flow cytometry, enzyme-linked immunosorbent assay, and immunohistochemistry. The binding competitiveness of novel anti-CD26 mAbs with the humanized anti-CD26 mAb YS110 was also examined.

Results: We have succeeded in developing novel anti-human CD26 mAbs suitable for immunohistochemical staining of CD26 in formalin-fixed tissue sections with reliable clarity and intensity. Importantly, some of these mAbs exhibit no cross-reactivity with the humanized anti-CD26 mAb.

Conclusions: These novel mAbs are potentially useful as companion diagnostic agents to analyze CD26 expression in the clinical setting while advancing future CD26-related research.

Virtual slides: The virtual slides for this article can be found here: http://www.diagnosticpathology.diagnomx.eu/vs/5987140221097729

Keywords: CD26/dipeptidyl peptidase 4, Immunohistochemical staining, Companion diagnostic drug, Malignant mesothelioma, T cell costimulation

* Correspondence: morimoto@ims.u-tokyo.ac.jp
[1]Department of Therapy Development and Innovation for Immune Disorders and Cancers, Graduate School of Medicine, Juntendo University, 2-1-1, Hongo, Bunkyo-ku, Tokyo 113-8421, Japan
Full list of author information is available at the end of the article

Introduction

CD26 is a 110-kDa type II membrane-bound glycoprotein with dipeptidyl peptidase IV (DPPIV) activity in its extra cellular domain [1-3]. CD26 is composed of 766 amino acids (AAs), and is anchored to the lipid bilayer by a single hydrophobic segment at residues 7–28. The cytoplasmic tail of CD26 is composed of only 6 amino acid residues at the N-terminal end (AA 1–6) without a common signaling motif structure. The predominant part of CD26 consists of the extra cellular domain (AA 29–766) divided into three regions, a glycosylated region, a cysteine-rich region and a C-terminal DPPIV catalytic region [4,5]. DPPIV belongs to the serine protease family, able to cleave dipeptides from polypeptides with N-terminal penultimate proline or alanine, and regulates the activities of a number of cytokines and chemokines [3]. CD26 is a multifunctional molecule associated with various proteins such as adenosine deaminase (ADA), caveolin-1, CXCR4, collagen, and fibronectin, and is expressed on various cell types, including epithelial cells (kidney proximal tubules, bile duct, prostate and intestine), endothelial cells as well as T lymphocytes [4-6]. The function of CD26 is dependent on cell types and the microenvironment, which influence its multiple biological roles [4-7].

In addition to being a marker of T cell activation, CD26 is associated with T cell signal transduction processes as a costimulatory molecule [4]. While CD26 expression is increased following activation of resting T cells, $CD4^+CD26^{high}$ T cells respond maximally to recall antigens such as tetanus toxoid [8]. Moreover, crosslinking of CD26 and CD3 with solid-phase immobilized monoclonal antibodies (mAbs) can induce T cell costimulation and IL-2 production by $CD26^+$ T cells [4]. Furthermore, high CD26 cell surface expression in $CD4^+$ T cells is correlated with the production of T_H1-type cytokines and high migratory activity [4]. Taking into account the data that effector T cells in inflamed lesions express high levels of CD26, it is conceivable that $CD4^+CD26^+$ T cells play an important role in the inflammatory process [5,9,10]. We have recently found that cytotoxic activity of $CD8^+$ T cells is also regulated via CD26-mediated costimulation [11]. More recently, we have shown that humanized anti-CD26 mAb appears to be a promising novel therapy for the clinical control of graft-versus-host disease (GVHD) in a xenogeneic GVHD murine model [12]. CD26 is also expressed on various tumors such as malignant mesothelioma, renal carcinoma, colon cancer, hepatocellular carcinoma, lung cancer, prostate cancer, gastrointestinal stromal tumor (GIST), thyroid cancer, T-lymphoblastic lymphoma and T-acute lymphoblastic leukemia [13]. We have shown that administration of anti-CD26 mAb resulted in both in vitro and in vivo inhibition of tumor cell growth, migration and invasion, and enhanced survival of mouse xenograft models inoculated with T-lymphoma, renal cell carcinoma or malignant mesothelioma [14-16]. Based on these findings, we have focused on CD26 as a novel therapeutic target for various tumors and immune disorders, and have developed a humanized anti-CD26 mAb, YS110, which is being investigated currently in a phase I clinical trial for patients with CD26-expressing tumors, including malignant mesothelioma [17].

The development of companion diagnostic agents to be used in conjunction with the appropriate therapeutic modalities is essential to maximize therapeutic effectiveness while minimizing associated toxicities. Detection of tumor CD26 expression is critical to determining potential eligibility for treatment with humanized anti-CD26 mAb, and it is also important to determine whether CD26 expression on tumors or lymphocytes is affected by anti-CD26 mAb therapy. Immunohistochemical staining of CD26 with the many anti-CD26 mAbs previously developed in our laboratory [18] did not reveal an anti-CD26 mAb that can clearly detect the denatured CD26 molecule in formalin-fixed paraffin-embedded tissues. Meanwhile, testing of several commercially available anti-CD26 mAbs designated as research reagents for immunohistochemical staining, and a mAb purchased from MBL indicated that these mAbs could stain the denatured CD26 in formalin-fixed tissues, but not with sufficient clarity. On the other hand, our testing of commercially available anti-CD26 polyclonal antibodies (pAbs), and a pAb purchased from R&D Systems showed that these reagents exhibited reliable staining pattern and intensity [19]. However, the disadvantage of pAbs is the potential lot-to-lot variability in staining pattern and intensity, which makes pAbs not the ideal reagents for diagnostic testing of patient specimens in the clinical setting, where consistency and uniformity are required.

In the present study, by immunizing mice with CD26 protein denatured in urea buffer, we have succeeded in developing novel anti-human CD26 mAbs that can be used as companion diagnostic reagents suitable for immunohistochemical staining of CD26 in formalin-fixed tissue sections with reliable clarity and intensity. In addition, since some of these mAbs display no cross-reactivity with the therapeutic humanized anti-CD26 mAb, they may be suitable for assays analyzing CD26 expression during or following treatment with the humanized anti-CD26 mAb.

Materials and methods

Animals

Female BALB/c mice were purchased from CLEA Japan (Tokyo, Japan) and housed in a specific pathogen-free facility in micro-isolator cages. Animal experiments were